THE JOURNAL OF PHYSICAL CHEMISTRY B

Article

pubs.acs.org/JPCB

Long-Range Electron Transfer with Myoglobin Immobilized at Au/Mixed-SAM Junctions: Mechanistic Impact of the Strong Protein Confinement

Dimitri E. Khoshtariya,*[,†,‡,§] Tinatin D. Dolidze,[†,‡,§] Mikhael Shushanyan,[†,‡,§] and Rudi van Eldik*[,†]

[†]Department of Chemistry and Pharmacy, University of Erlangen-Nürnberg, 91058 Erlangen, Germany

[‡]Institute for Biophysics and Bionanosciences at the Department of Physics, I. Javakhishvili Tbilisi State University, 0128 Tbilisi, Georgian Republic

[§]Department of Biophysics, I. Beritashvili Center for Experimental Biomedicine, 0160 Tbilisi, Georgian Republic

ABSTRACT: Horse muscle myoglobin (Mb) was tightly immobilized at Au-deposited ~15-Å-thick mixed-type (1:1) alkanethiol SAMs, HS−$(CH_2)_{11}$−COOH/HS−$(CH_2)_{11}$−OH, and placed in contact with buffered H_2O or D_2O solutions. Fast-scan cyclic voltammetry (CV) and a Marcus-equation-based analysis were applied to determine unimolecular standard rate constants and reorganization free energies for electron transfer (ET), under variable-temperature (15−55 °C) and -pressure (0.01−150 MPa) conditions. The CV signal was surprisingly stable and reproducible even after multiple temperature and pressure cycles. The data analysis revealed the following values: standard rate constant, 33 s^{-1} (25 °C, 0.01 MPa, H_2O); reorganization free energy, 0.5 ± 0.1 eV (throughout); activation enthalpy, 12 ± 3 kJ mol^{-1}; activation volume, −3.1 ± 0.2 cm^3 mol^{-1}; and pH-dependent solvent kinetic isotope effect (k^0_H/k^0_D), 0.7−1.4. Furthermore, the values for the rate constant and reorganization free energy are very similar to those previously found for cytochrome *c* electrostatically immobilized at the monocomponent Au/HS−$(CH_2)_{11}$−COOH junction. In vivo, Mb apparently forms a natural electrostatic complex with cytochrome b_5 (cyt-b_5) through the "dynamic" (loose) docking pattern, allowing for a slow ET that is intrinsically coupled to the water's removal from the "defective" heme iron (altogether shaping the biological repair mechanism for Mb's "met" form). In contrary, our experiments rather mimic the case of a "simple" (tight) docking of the redesigned (mutant) Mb with cyt-b_5 (Nocek et al. *J. Am. Chem. Soc.* **2010**, *132*, 6165−6175). According to our analysis, in this configuration, Mb's distal pocket (linked to the "ligand channel") seems to be arrested within the restricted configuration, allowing the rate-determining reversible ET process to be coupled only to the inner-sphere reorganization (minimal elongation/shortening of an Fe−OH_2 bond) rather than the pronounced detachment (rebinding) of water and, hence, to be much faster.

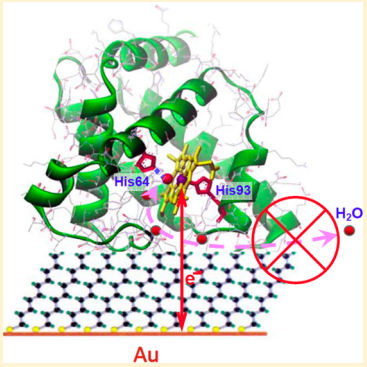

INTRODUCTION

Historically, globins (mostly myoglobins of different origin) have been introduced as typical representatives of smaller globular proteins to study their structure, dynamics, and function and the links between these three fundamental aspects.[1−5] A broad spectrum of intraglobular, hierarchically networked space- and time-spanned conformational transformations have been recognized to determine the functional properties, which, for diverse globins, entail small-ligand storage and transport,[1−3,6,7] "reparative" (outer-sphere) electron transfer (ET),[7−10] molecular catalysis (enzymatic activity),[1,11,12] and so on. However, the relative ease of exposing of well noticeable conformational motifs has usually been counterbalanced by the richness of their manifold, hence giving rise to difficulties in profound mechanistic comprehension.[3]

Specifically, in mammals, myoglobin (Mb) [as well as hemoglobin (Hb)] binds oxygen (O_2) in the reduced (Fe^{2+}) state, but under physiological conditions, it can unintentionally be oxidized to the O_2-inactive state (Fe^{3+}).[8,9] In vivo, the globins' reparation apparently takes place by the help of soluble cytochrome b_5 (cyt-b_5) which reduces Fe^{3+}Mb (or Fe^{3+}Hb) back to the active Fe^{2+} state by interprotein (outer-sphere) ET.[8−10,13−17] In the oxidized (ferric) Fe^{3+} state, globins in their distal pockets have a water molecule covalently bound to the heme iron (forming the "met" form), with water being simultaneously hydrogen-bonded to the imidazole group of a distal His-64. In the reduced (ferrous) Fe^{2+} state, H_2O does not bind to the heme iron but can probably retain the hydrogen bond to His-64.[18−34] Detachment of water from the heme iron and its subsequent intraglobular diffusion, presumably through the hydrogen-bonded aqueous network (through the so-called "ligand channel", vide infra), should be a prerequisite for the ultimate penetration of O_2 into the distal pocket and binding to Fe^{2+}.[8,9,34−38] Indeed, when small "gaseous" ligands such as O_2, CO, or NO bind to the ferrous iron atom in Fe^{2+}Mb, the distal pocket water must be displaced beforehand. Hence, the Fe^{3+}/

Received: October 13, 2013
Revised: December 20, 2013
Published: December 26, 2013

Fe^{2+} redox process (implying the outer-sphere ET pattern) in globins is essentially coupled to a naturally occurring detachment of the water molecule from the heme and, obviously, to a substantial reorganization of the nearest environment [e.g., the conformational displacement of a His-64 side group with imidazole hydrogen-bonded to a given water, hopping of water molecules within the associated intraglobular water chain, opening of the protein's ligand channel (gate); see refs 35−44, vide infra]. The mechanistic issue of coupling between the outer-sphere ET and water displacement, has been investigated by several experimental and theoretical approaches:

In their earlier work, Parak et al.[39−42] reduced the high-spin metmyoglobin ($Fe^{3+}MbH_2O$) by either X-irradiation (reduction by thermalized electrons) or dye-mediated photoinduced ET at cryogenic temperatures. Formation of the "metastable" low-spin $Fe^{2+}MbH_2O$ configuration was observed by means of X-ray diffraction and Mössbauer and optical spectroscopies, with H_2O still covalently bound to Fe^{2+}. Upon heating above 140 K, this species transformed into the conventional ("stable") high-spin Fe^{2+}Mb ("deoxy") form, with H_2O somewhat moved away from Fe^{2+}.[39−42] Hence, under these cryogenic conditions, the ligand water can attain only three fixed positions at (near) heme iron, rather than diffuse through the ligand channel.

Different groups have applied electrochemical techniques to study the redox response of a native or chemically modified Mb in a freely diffusing regime[43−49] and demonstrated that chemical alterations that presumably destroy a water chain within the ligand channel (hence, blocking the detachment and migration of water from the heme iron) lead to the essential increase in the ET rate constant. Other electrochemical studies have exploited the redox properties of Mb in a surface-confined regime[50−54] and found that the ET rate is essentially determined by the confinement mode.

As briefly mentioned above, Hoffman and co-workers[13−17] extensively studied "homogeneous" (liquid-phase) ET between cyt-b_5 and the native and mutant forms of Mb and demonstrated that the wild protein forms a rather loose precursor complex with cyt-b_5 (the case of a "dynamic docking") and then undergoes relatively slow interprotein ET. The proper re-engineering of the protein surface might lead the tight protein−protein complexation (the case of a "simple docking") and the essentially improved ET rate constant.[16,17]

Very recently, by connecting the two earlier approaches, Bowden et al.[55,56] considered links between the protein−protein and protein−SAM docking paradigms (implying liquid-phase and interfacial assemblies, respectively) in the context of the impact of the docking strength on Mb's functional ability. They reported voltammetric studies on dehydroperoxidase (monomeric bacterial globin[57]) long-range ET at Au electrodes modified by thicker mixed (−COOH/−OH)-terminated SAMs.[55,56] The subsequent analysis led to the necessity of considering the role of the protein's conformational dynamics in ET. A similar tentative conclusion was drawn in our preliminary short communication[58] reporting voltammetric studies of ET for horse muscle Mb tightly bound to mixed $HS-(CH_2)_{11}-COOH/HS-(CH_2)_{11}-OH$ SAMs.

Furthermore, advanced theoretical modeling[59−63] and molecular dynamic simulations[64−66] were performed to comprehend Mb mechanisms at the atomistic level. In particular, notions of the generalized ("multidimensional") theory of charge transfer[67−71] (encompassing the basic Landau−Zener energy-curve-crossing paradigm) were addressed to understand coupling of the ligand attachment/detachment reaction coordinate with the heme/protein degrees of freedom.[59−66] Almost in parallel, notions of the same general theory were applied for the mechanistic analysis of ET (electron-exchange) coupling with recognizable intramolecular (inner-sphere) and solvent (outer-sphere) vibrational modes in model metal complexes such as $[Fe(H_2O)_6]^{2+/3+}$.[72−76] However, no attempts have been made so far to treat all of the elementary events involving metmyoglobin, including the water ligand dynamics and outer-sphere ET, within a unified combined model based on the generalized multidimensional theory.[67−71]

In this article, we present a complete account of our original work on Mb film voltammetry at mixed, tightly grasping Au/SAM junctions, including the effects of temperature, pressure, and solvent isotope substitution. Our results indicate very strong docking of Mb that, seemingly, severely restricts the ligand channel opening and, hence, any sizable detachment of water from the heme iron (resembling the case with a frozen environment[39−42]). In terms of contemporary theoretical notions, "ligand water" in this particular system acts as stable ligand, undergoing minor inner-sphere reorganization upon electron exchange, and this fact leads to accelerated ET rate constant (compared to the case of "free" Mb, in which ET can be coupled to the longer jump of a ligand water inside Mb's distal pocket) approaching that of cyt-*c* under comparable experimental conditions.

EXPERIMENTAL SECTION

Materials. Higly purified Mb from horse skeletal muscle was purchased from Sigma and used as received. The alkanethiols 12-mercaptopropionic acid and 11- mercaptoundecanol, of the highest purity commercially available, were from Sigma-Aldrich and used as received. Deuterium oxide was obtained from Euriso-top C.E. Saclay Gif-sur-Yvette, France. Tris-(hydroxymethyl)aminomethane hydrochloride (Tris-HCl, 98%; Sigma) buffers, which are known to withstand pressure-induced pH changes,[77] were used in the high-pressure experiments, at pH/pD 7.3, as well as in the variable-temperature (pH/pD 7.3) and variable-pH (5.6−7.3; T = 25 °C, ambient pressure) experiments, to guarantee comparable experimental conditions. In addition, phosphate buffers were used to allow for a further pH (pD) variation within the range of 7.3−8.5. Working solutions (20 mM Tris or phosphate) were prepared by dissolving the buffer components in Milli-Q water or commercial D_2O. Correspondingly, the pH or pD values for the working solutions were adjusted by addition of H_2O- or D_2O-based concentrated solutions of NaOH or HCl. [See refs 78−81 regarding the comparison of pH and pD scales, as well as the corresponding subsection in Results and Discussion.]

Electrochemical Cell and Electrode Preparation. The high-pressure electrochemical cell and vessel were described in detail before.[82−87] In brief, the working electrode (Ø 1.6-mm gold disk sealed in Teflon cylinders, BAS), auxiliary electrode (platinum wire), and quasireference electrode (Ag/AgCl/4 M KCl) were sealed into the cell cap by two O-rings. The assembled pressure vessel containing the cell was placed in a thermostatted water jacket equilibrated at the desired temperature. The temperature was controlled to within ±0.1 °C using a digital temperature controller. Working solutions were thoroughly purged with argon (for ca. 30 min) before kinetic

dx.doi.org/10.1021/jp4101569 | J. Phys. Chem. B 2014, 118, 692−706

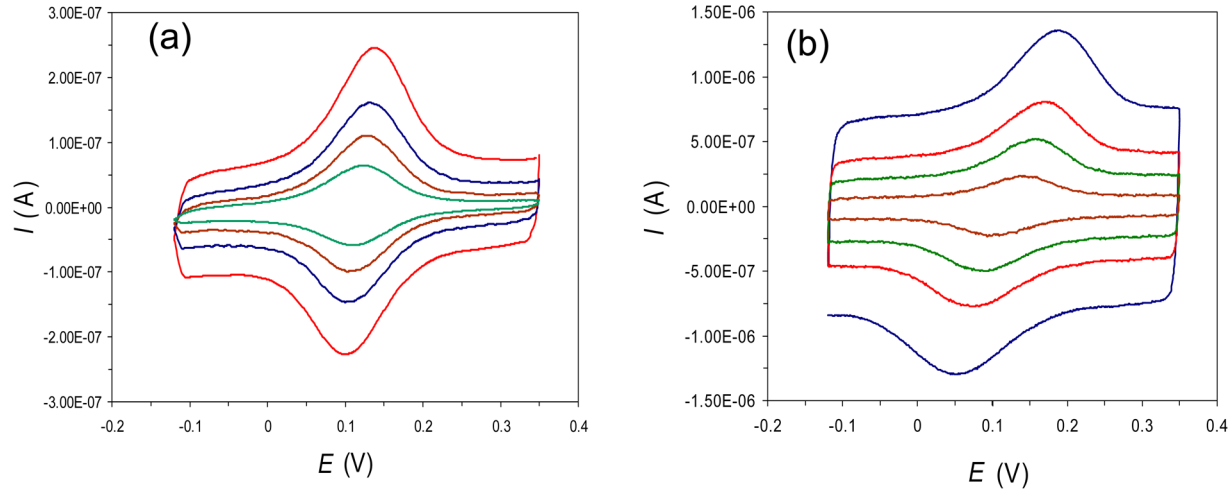

Figure 1. Typical cyclic voltammograms for the Mb electron exchange at Au/SAM junctions composed of the mixed (1:1) alkanethiol elements HS−$(CH_2)_{11}$−COOH and HS−$(CH_2)_{11}$−OH. Potential scan rates: (a) 0.3, 0.5, 0.7, and 1 V s^{-1} (H_2O, phosphate buffer, pH 7.3, 25 °C); (b) 1, 2, 3, and 5 V s^{-1} (D_2O, Tris buffer, pH 7.7, 50 °C).

Table 1. Kinetic and Activation Parameters of ET (Electron Exchange) for Mb Immobilized at a 1:1 Mixed HS−$(CH_2)_{11}$−COOH/HS−$(CH_2)_{11}$−OH SAM (H_2O and D_2O Solutions) and at the Monocomponent HS−$(CH_2)_{11}$−COOH SAM, along with the Available Data for Cyt-*c* Immobilized at the Same Monocomponent SAM

protein, SAM type	k^0 (s^{-1}) (20 °C, 0.1 MPa)	λ (eV)	ΔH_a (kJ mol^{-1})	ΔV_a (cm^3 mol^{-1})
Mb, mixed SAM (H_2O)	33 (pH 7.3)	0.5 ± 0.1	12.1 ± 0.3	−3.1 ± 0.2
Mb, mixed SAM (D_2O)	38 (50)[a] (pD 7.3)	0.5 ± 0.1	11.2 ± 0.5	−3.6 ± 0.3
Mb, mono SAM (H_2O)	8 (pH 7.3)	not measurable	not measurable	not measurable
cyt-*c*, mono SAM (H_2O)	36[b] (pH 7.0)	0.4−0.6[c]	14.4[c]	−5.5[d]

[a]Value from a particular experimental series on the impact of T and P on k^0. [b]Data from ref 114. [c]Data for cyt-*c* attached to the Py-terminated SAM from refs 92 and 109. [d]Data for freely diffusing cyt-*c* from ref 83.

experiments to remove the oxygen. The variable-pressure measurements were performed starting at P = 5 MPa (to eliminate any small bubbles) in steps of 50 MPa. The variable-temperature measurements were performed with temperature steps of 10 K.

The gold disk electrode, used as SAM-deposited substrates in bioelectrochemical kinetic experiments, was treated according the procedures described elsewhere.[85] In brief, the electrode surface was cleaned with successive exposure to 60 °C sulfochromic acid and 5% HF. This procedure was repeated three times. Mono-component and mixed self-assembled monolayers were prepared by direct immersion of freshly cleaned electrodes into single-component and mixed (1:1) ethanol solutions of the corresponding 5×10^{-3} M alkanethiols for 24 h. The electrodes were kept in the coating solutions overnight to allow complete formation of SAM films. For protein immobilization, SAM-modified electrodes were thoroughly rinsed with ethanol, Milli-Q water, and finally buffer solution and were transferred into 20 mM Tris (or phosphate) buffer solution containing 1 mg mL^{-1} Mb for up to 30 min. All potentials are given versus Ag/AgCl/3 M NaCl.

Instrumentation and Measurements. Electrochemical measurements were carried out with an Autolab Electrochemical Analyzer PGSTAT 30, equipped with the General Purpose Electrochemical System (GPES) software for Windows (version 4.9). Conventional fast-scan cyclic voltammetry (CV) was applied for the determination of the standard unimolecular kinetic constant (k^0) by plotting the deviations of the cathodic (E_{Pc}) and anodic (E_{Pa}) CV peak positions from the formal redox potential, $E^0 = (E_{Pc} + E_{Pa})/2$ ($\Delta E = |E_{Pc} - E^0| \approx |E_{Pa} - E^0|$) versus the reduced potential scan rate, through the established procedures[88−90] (see also refs 86, 87, and 91−93 and the next subsection). Autolab software was used for a variety of data analyses and the corrections of the experimental CV response for "postmeasurement" ohmic potential drop (IR_Ω, where R_Ω is the solution resistance between the reference and working electrodes),[86,87] when needed. The values of R_Ω at different temperatures were calculated taking into account the changes in conductivity of the solution with temperature.

The surface coverage of electrochemically active Mb (Γ) was determined using the area under the peak of the CV curve (θ) according to the equation[94]

$$\Gamma = \theta/nFS\nu \quad (1)$$

where n is the number of transferred electrons, F is the Faraday constant, S is the geometric area of the electrode, and ν is the potential scan rate. The value of Γ for Mb at mixed-SAM-modified gold electrodes (T = 25 °C, ambient pressure) was, on average, $(4 \pm 1) \times 10^{-12}$ pmol cm^{-2}.

CV Data Analysis. Figure 1 shows representative cyclic votammograms recorded for Mb films immobilized at Au/SAM junctions composed of the mixed-type (1:1) alkanethiol elements, HS−$(CH_2)_{11}$−COOH and HS−$(CH_2)_{11}$−OH. The CV signal was surprisingly stable and reproducible for many hours, even after multiple temperature and pressure cycles within the ranges 15−55 °C or 0.01−150 MPa, respectively. In contrast, in the case where the monocomponent Au/SAM junctions made solely of the HS−$(CH_2)_{11}$−COOH element

dx.doi.org/10.1021/jp4101569 | J. Phys. Chem. B 2014, 118, 692−706

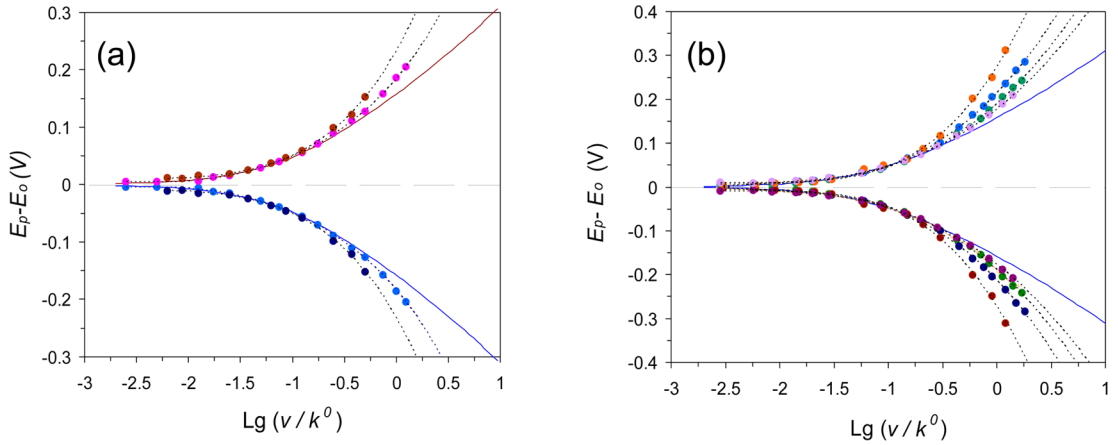

Figure 2. Data fittings for CV peak deviations from the midpoint potential as a function of the scaled scan rate (points) by the Marcus model with λ = 0.5 ± 0.1 eV (solid lines): (a) D_2O; pH-meter reading 6.4 (phosphate buffer), 25 °C; pressure 0.1 and 150 MPa, respectively. (b) Different Mb samples (within a purchase time gap of one year) under different buffering (phosphate vs Tris buffer) and pH (6.0–8.0) conditions (25 °C, 0.1 MPa). Dashed curves are drawn solely for purpose of guiding the eye (see text for more details).

were applied, an electrochemical CV signal similar to that depicted in Figure 1, appeared (not shown), but was much weaker, displayed a much lower value of the rate constant (see Table 1 and discussion below), and tended to disappear within approximately 30 min. Obviously, the reason for this dramatic divergence is the difference in morphology between the surfaces for these two types of SAMs, namely, the lower charge density for the mixed SAM compared to the monocomponent one. Indeed, according to Liang et al.,[13] for Mb, the protein surface area surrounding the partially exposed heme edge (presumably responsible for Mb docking) is not uniformly positively charged; hence, along with the additional possibility of a slight divergence in the SAM components' length, this factor leaves vast room for the variation in protein/SAM binding (grasping) efficiency (see, e.g., ref 93 on a similar issue).

Marcus equation analysis was applied throughout to determine values of monomolecular standard rate constants and reorganization free energies of ET. In liquid electrolytes, Marcus theory[67,70] and its basic extensions (see refs 68, 69, 71, and 95–99) are commonly used to describe electrochemical charge-transfer rates in both the weak- and strong-electronic-coupling limiting cases. In general form, the reduction and oxidation rate constants can be expressed by the equations[88−91]

$$k_{red}(\xi) = A \int \exp\left\{-\frac{[(\varepsilon_F - \varepsilon) + e\xi + \lambda_0]^2}{4\lambda_0 RT}\right\}[f(\varepsilon)]\,\frac{d\varepsilon}{RT} \quad (2)$$

$$k_{ox}(\xi) = A \int \exp\left\{-\frac{[(\varepsilon_F - \varepsilon) - e\xi + \lambda_0]^2}{4\lambda_0 RT}\right\}[1 - f(\varepsilon)]\,\frac{d\varepsilon}{RT} \quad (3)$$

In eqs 2 and 3, λ_0 is the overall (resulting) reorganization energy of the system (vide infra), ξ is the overpotential (equal to the applied potential relative to the formal potential of the redox molecule), ε_F is the Fermi energy (equal to the applied potential), $f(\varepsilon)$ is the Fermi function, R is the gas constant, T is absolute temperature, and A is a pre-exponential factor whose form is specific for the intrinsic ET mechanism. The term ε is an integration variable that corresponds to the energy of the electronic levels in the electrode.

RESULTS AND DISCUSSION

Noticeable Deviations from the Marcus Model. Panels a and b of Figure 2 depict representative fitting patterns applied for the CV data obtained under different experimental conditions (different pressure, buffer composition, pH). One can see that the CV data within the overvoltage ranges up to ca. 0.1 eV (ca. 10 kJ mol^{-1}) can be almost perfectly fitted by the procedure based on the classical Marcus equation.[88−91] However, the data outside this range cannot be fitted by any theoretical curve of the Marcus model, which seemingly is an indication of nonparabolic shapes for free energy wells that present the ET energetics.[87,100−106] Importantly, the observed deviations cannot be attributed to the effects of uncompensated resistance, as the respective inputs for systems in the present study were found to be small and fully removable through the standard procedures (see the Experimental Section). The solid lines in both panels of Figure 2 correspond to a theoretically predicted situation with a Marcus reorganization free energy (λ_0) of 0.5 ± 0.1 eV (implying parabolic shapes of respective free energy wells). The relatively large error of ca. 20% comes from the limited overpotential ranges in which the data still match the Marcus model (vide infra).

It is natural to assume that, for the composite, slowly relaxing environments such as hydrated proteins additionally confined within semirigid films, the resulting (effective) Gibbs energy wells that shape, λ_0, are almost equally contributed by the fast, statistically independent harmonic modes and by slow, cooperatively relaxing (dissipative) modes, where the latter are liable to inharmonic alterations (see the next subsection for more details). Under zero- or small-energy-gap conditions, seemingly, both of them tend to display the linear or at least quasilinear medium response pattern.[100−107] However, at higher overpotentials, the high-energy, nonparabolic limbs of the ET-coupled conformational energy wells begin to participate at the curve-crossing point of the resulting free energy wells, which would unavoidably result in deviations from Marcus-type fitting curves,[87,100−106] as depicted by Figure 2. Furthermore, one should note that application of Marcus analysis for a limited range of experimental data collected at

dx.doi.org/10.1021/jp4101569 | J. Phys. Chem. B 2014, 118, 692−706

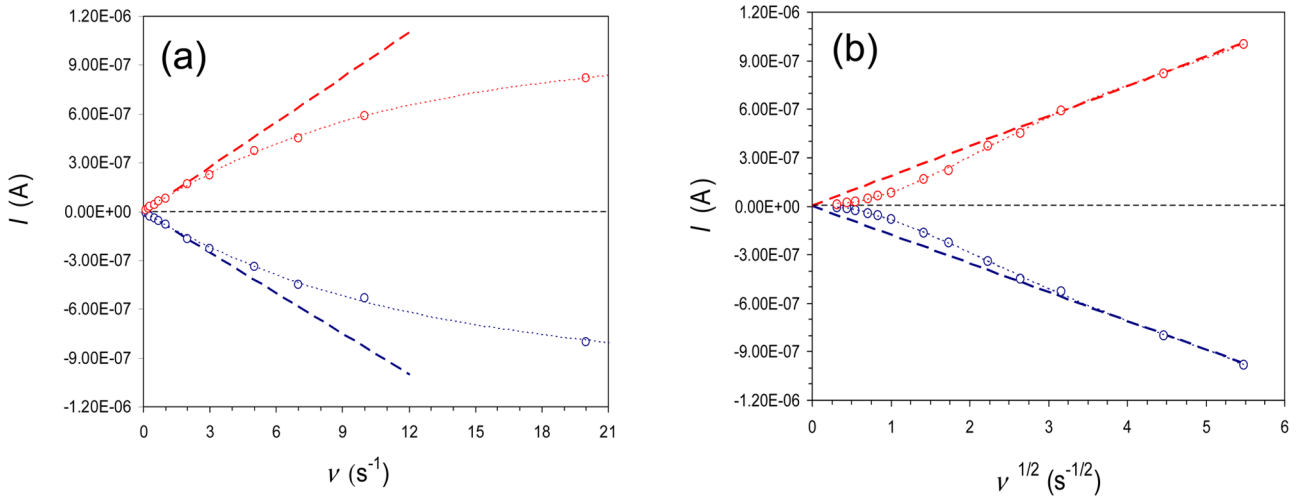

Figure 3. Dependencies of peak currents for Mb electron exchange at Au/SAM junctions as functions of the (a) potential scan rate and (b) square root of the potential scan rate. The bold dashed straight lines indicate mechanistic matches for the "diffusion-free" and "diffusion-related" regimes.

lower overvoltages (up to ca. 0.1 eV) is well justified provided that the values of the thus-determined standard rate constants and reorganization free energies are considered as effective ones (having physical meaning at lower energy gaps), that is, the rate constants at large overpotentials (energy gaps exceeding ca. 0.1 eV) cannot be calculated using this value of the reorganization energy (vide infra). One can see that, below ca. 0.1 eV, the CV data collected under very different experimental conditions can be fitted by an almost "universal" theoretical curve signifying the common value of λ_0 (0.5 ± 0.1 eV; Figure 2). However, the values for rate constants under different conditions certainly are different (see Table 1). The CV behavior at large overvoltages (Figure 2b) was different for two Mb samples with the same specifications, purchased within a one-year interval. This might be an indication that the contribution of individual harmonic (presumably "fast") reorganizable modes is much more reproducible from sample to sample than that from much "slower", partially unharmonic modes, representative of the protein's and SAM's collective fluctuations (much more prone to variations caused by intrinsic sample-to-sample variations or external physical or chemical factors), vide infra.

Recently, Mie et al.[48] reported on the large "inverted" solvent H_2O/D_2O kinetic isotope effect (KIE) of 0.13 for wild-type porcine Mb reacting at an In_2O_3 electrode in a freely diffusing regime (pH 6.5, phosphate buffer). This large KIE was eliminated by means of modifications of the distal histidine (His-64) through either mutation or chemical treatment by BrCN. These modifications are also known to improve ET rate constant, along with the electrochemical performance, reversibility, and reproducibility.[43−48] Based on the previous results, the authors of ref 48 explained their findings on the KIE interplay in terms of the involvement of a water molecule bound to the heme iron of the intact Mb in its oxidized form (forming metmyoglobin) and its dissociation and reassociation accompanying Fe reduction and reoxidation. This process presumably is accompanied by substantial reorganization of the hydrogen-bonded network around the distal pocket involving the protein's slow collective (conformational) modes.[87,100−107] Mutational replacement of distal histidine or its chemical modification by BrCN seemingly prevents the heme group from binding water because of the lack of the necessary stabilizing interaction, leaving the heme iron structure five-coordinated (forming so-called deoxymyoglobin).[39−42] This, in turn, prevents the distal pocket area from large-scale energy-consuming collective restructuring, making the resultant ET process detangled from the reorganization of excess inner-sphere ($Fe-OH_2$) and related conformational modes and, hence, much faster (vide infra).

Coupling of ET to "Mobile" Water and Heme/Protein Dynamics. In the long-range, nonadiabatic (NA) ET regime (see refs 68−71, 83, 86, 88−93, and 108−110), the pre-exponential factor can be written as

$$A = A_{NA} = \frac{V_{AB}^{\ 2}}{\hbar}\rho_m\sqrt{\frac{\pi^3 RT}{\lambda_0}} \tag{4}$$

where V_{AB} is the electronic coupling between the electron-donor and -acceptor states and ρ_m is the density of electronic states in the metal (electrode). Other symbols were defined above. The standard electron-transfer rate constant, k^0, can be obtained from either eq 2 or 3. Within the NA limit, where $V_{AB} \ll RT$ (or λ_0), and when the overpotential is zero, so that the ET is controlled by exchange at the electrode Fermi level, eqs 2 and 3 simplify to (see refs 68−71, 83, 86, 88−93, and 108−110)

$$k^0 = A\ \exp\left(-\frac{\Delta G_a}{RT}\right) \tag{5}$$

where, within the harmonic approximation for Gibbs energy wells, in a general case, the following approximation is applicable (see, however, the discussion below on restrictions on the harmonic approximation for the current case)

$$\Delta G_a = \frac{(\Delta G_0 + \lambda_0)^2}{4\lambda_0} \tag{6}$$

in which ΔG_0 is the free energy gap (matching the overvoltage, $e\xi$; see eqs 2 and 3). Further, in the case of zero overvoltage (condition for the determination of the standard rate constant, k^0), eq 6 simplyfies to $\Delta G_a = \lambda_0/4$.

In the case of complex redox-active systems, such as the confined protein, the slow modes of the protein's immediate environment, the protein/water interfacial zone, the protein matrix, and even the protein's metal core (heme) can essentially be coupled and, as already mentioned above, form hierarchi-

dx.doi.org/10.1021/jp4101569 | J. Phys. Chem. B 2014, 118, 692−706

cally organized networks (see refs 2−5, 34−38, 59−61, 87, 100−103, and 107). Certainly, the heme modes involved in the spin inversion event (if it occurs) and remote proton translocations disclosed through the KIE definitely are involved as individual and/or collective reorganizable modes (vide infra).

Figure 3 displays the dependencies of peak currents for Mb electron exchange at Au/mixed-SAM junctions against the potential scan rates in two different ways. Figure 3a displays the peak current directly as a function of the potential scan rate, whereas Figure 3b shows it as a function of the square root of the potential scan rate. In the "classical" case of tightly (irreversibly) immobilized redox-active species, a linear dependence in Figure 3a could be expected, whereas in the "classical" case of a freely diffusing redox couple, a linear dependence in Figure 3b is anticipated.[111] Obviously, formally, both patterns are encountered. Because Mb detachment from the SAM surface is excluded (as checked by control experiments after each small and large cycling experiment, implying cycling versus scan rate and versus temperature and pressure), some intrinsic mechanistic complication can be outlined. Behavior similar to that shown in Figure 3b was observed by Bowden et al.[55,56] for the case of mixed-SAM-immobilized bacterial globin and ascribed to the manifestation of the conformational aspect, implying the depletion of the redox-active globin fraction with increasing scan rate; namely, it is assumed that some globin fractions are tightly fixed such that the accompanying conformational transformation cannot follow the scan rate and, hence, cannot allow for ET. Consequently, more tightly bound fractions of Mb are increasingly turned off. Interestingly, the pattern transition from type a to type b (Figure 3) correlates with the pattern transition depicted in each panel of Figure 2, from a pattern that can be fitted by the Marcus model, that is, by the trumpet-like function resembling the medium's linear response (parabolic free energy surfaces), to the pattern where such a fitting is impossible (see ref 87 for another example). In the framework of the hypothesis proposed by Bowden et al.,[56] an observed correlation between the anomalies regarding the CV peak current and peak potential patterns (both exposed at higher potential scan rates), at first glance, do not seem controversial. However, as higher overpotentials (which, in general, favor the overall ET process) are attained at higher scan rates, it becomes unclear why ET for some Mb fractions should be entirely blocked. Instead, some other, more delicate complication should be operative here.

In a previous article,[87] we interpreted the anomalous appearance of trumpet-like curves similar to those depicted in Figure 2a,b as due to a violation of the medium's linear response archetypal model (involvement of nonparabolic fragments of corresponding free energy reaction curves). We also recall the pattern depicted in Figure 3b realized at relatively high scan rates, which, within the traditional CV analysis,[111] should be associated with reactant diffusion, in contrast to the pattern in Figure 3a, which is typical for the surface-confined ET process. A changeover between these two patterns has previously been observed for a number of interfacial processes, with the immobilized species involved in ET coupled to the diffusional motion of another reactant, for example, a proton (note the well-documented case of the surface confined glucose oxidase[112,113]). Although, in contrast to the case of glucose oxidase,[112,113] in our case, ET is presumably coupled only to remote proton transfers (vide infra), at higher scan rates when higher overvoltages are attained, diffusion of protons through the protein matrix, which should, in turn, be coupled to the conformational degrees of freedom, might become a bottleneck component of the overall concerted process. Specifically, at high overpotentials, the high-lying fragments of ET-related free energy curves (essentially contributed by conformational modes) become progressively involved. Because the curvature of these fragments can, in general, deviate from the classical parabolic shape (in particular, be steeper at higher energy levels; see, e.g., refs 87 and 100−106), this might lead to the kinetic irregularities depicted in Figures 2 and 3.[87]

Figure 4 displays a logarithmic plot of a data collection including a logarithmic plot of the electron-exchange

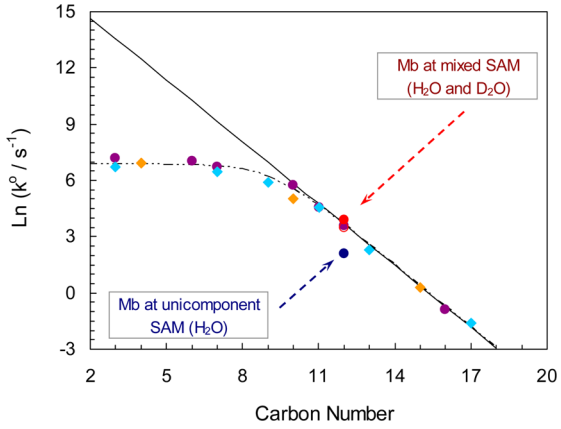

Figure 4. Logarithmic dependencies of rate constants of electron-exchange processes at alkanethiol SAM-coated Au electrodes for the following systems: cyt-*c* at HS−$(CH_2)_n$−COOH SAMs (violet circles),[109,114] azurin at HS−$(CH_2)_n$−CH_3 SAMs (sky blue and orange rhombi; see refs 86 and 110 for reviews), myoglobin at mixed HS−$(CH_2)_{11}$−COOH/HS−$(CH_2)_{11}$−OH SAMs (open and solid red circles; this work), and myoglobin at HS−$(CH_2)_{11}$−COOH SAMs (solid blue circle; this work), where the data for the two myoglobin systems are pointed out by the red and blue dashed arrows, respectively. See text for details.

unimolecular rate constants for cyt-*c* and azurin at Au electrodes coated by the monocomponent HS−$(CH_2)_n$−COOH[109,114] and HS−$(CH_2)_n$−CH_3[86,110] SAMs, respectively, with variable n (n = 3−17). The rate constants for Mb immobilized at the monocomponent HS−$(CH_2)_{11}$−COOH SAM and at the 1:1 mixed HS−$(CH_2)_{11}$−COOH/HS−$(CH_2)_{11}$−OH SAM (this work) are also displayed. Surprisingly, the value for the latter system coincides, within the experimental error, with that obtained for cyt-*c* at the monocomponent HS−$(CH_2)_{11}$−COOH SAM,[114] whereas the values for the reorganization free energies are also similar (Table 1).

The rate constant for Mb at the monocomponent SAM that could be measured within the limited time periods (because of Mb desorption) displayed a much smaller value (Table 1), notwithstanding the virtual similarity of ET distances for the monocomponent and bicomponent SAMs. These facts are indicative of the different steric/electrostatic interactional requirements for the Mb and cyt-*c* tight docking at the SAM terminal groups and the tunability of the SAM−Mb adsorption strength through the variation of the SAM composition. Our results also indicate that the ET efficiency for Mb essentially correlates with the degree of surface confinement (adsorption strength). The stronger the adsorption, the higher the ET rate constant. (However, note that, in general, the opposite trend occurs for a short-range, friction-controlled ET regime; see refs

dx.doi.org/10.1021/jp4101569 | J. Phys. Chem. B 2014, 118, 692−706

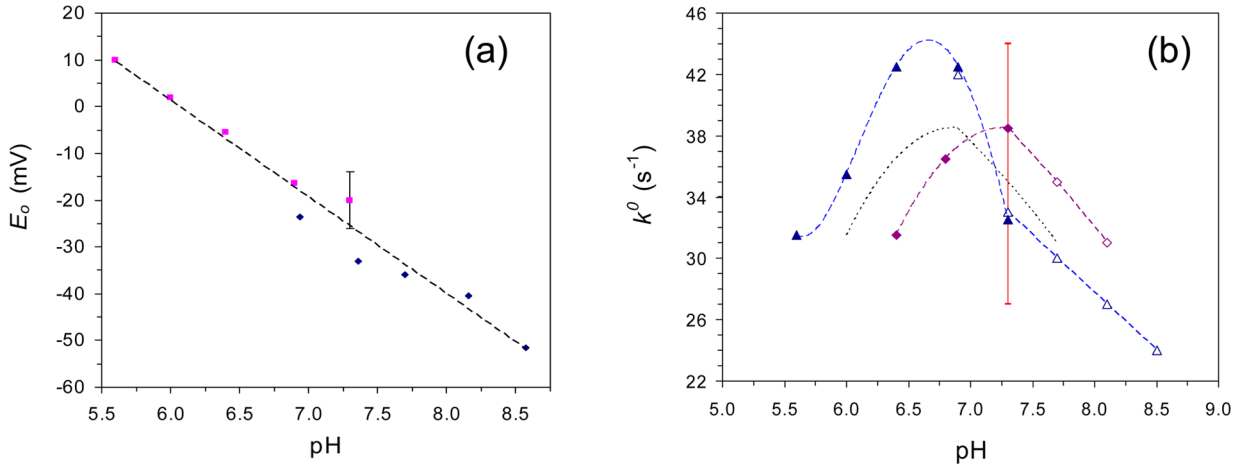

Figure 5. (a) Dependence of the CV midpoint (formal redox) potential of Mb electron exchange on pH: phosphate buffer, pink symbols; Tris buffer, dark blue symbols. (b) Dependencies of standard rate constants of Mb electron exchange, determined in buffered H_2O and D_2O solutions, on pH: phosphate buffer, solid symbols; Tris buffer, open symbols; H_2O solutions, triangles; D_2O solutions, rhombi. Dashed curves are drawn solely to guide the eye; violet symbols and corresponding dashed curve represent pD values determined for D_2O solutions, implying a 0.4 unit correction for the pH-meter reading; black dashed curve represents the same curve without correction (direct pH-meter reading); vertical red line indicates the pH value (7.3) at which the experiments for variable temperature and pressure were performed. See text for further discussion.

86, 87, 93, 109, and 110.) This conclusion is in accord with the recent work of Hoffman and co-workers[15−17] in which high rate constants of interprotein ET to Mb were achieved through the tightening of the protein−protein precursor docking complex. Recalling now results of other earlier studies in which, on one hand, different coupling regimes between ET and water displacement were demonstrated[43−45] and, on the other hand, two major (extreme) forms of Mb conformation (open vs closed) were established,[34,35] one might come to the logical conclusion that tight docking (i.e., external physical restriction of the conformation opening) leads to the restriction of normal water "detachment" from the heme group and subsequent intraglobular diffusion to the Mb exterior through the ligand channel, whereas loose docking allows it. Full water release should be coupled with the reduction of the metmyoglobin form by outer-sphere ET from the naturally occurring partner, cyt-b_5, through the loosely bound precursor complex, also allowing for water replacement by the key ligand, O_2.

Effects of Isotopic Composition (D_2O versus H_2O), pH (pD), Temperature, and Pressure. The values of the standard rate constants under different experimental conditions, determined through the above-described fitting procedure, and the corresponding activation parameters are collected in Table 1. Figure 5a depicts the dependence of the CV midpoint potential (i.e., the formal redox potential) on pH for Mb immobilized at Au-deposited mixed-type (1:1) HS−$(CH_2)_{11}$−COOH/HS−$(CH_2)_{11}$−OH films, whereas Figure 5b depicts the dependencies of the respective standard rate constants determined in buffered H_2O and D_2O solutions on pH (triangles), pD (rhombi), and uncorrected pH-meter reading in D_2O (black dotted curve without symbols; vide infra). The average slope for the first dependence, if considered linear, is ca. 20 mV per pH unit, which is much lower than the value expected for a simple equilibrium of a single proton transfer per transferred electron, namely, 59 mV per pH unit.[115] In the literature, for diversely arranged Mb layers, mostly larger slopes were reported (up to 50 mV, at the maximum), but always less than the theoretical value.[50−54] The noninteger values normally imply that a series of acid−base equilibria, rather than a single equilibrium, might fractionally contribute to E_0.[33] Generally speaking, several histidine groups of Mb displaying similar pK_a values might contribute. According to Cooper et al.,[33] these residues are likely to be not the proximal or distal histidines but rather the remote ones. It seems that protonic equilibria are only weakly coupled to ET in Mb, and the type of the Mb confinement might notably affect this coupling.

Inspection of Figure 5b indicates that the KIE magnitude, and even the aspect of its inversion, essentially depends on a consistent choice of the pD scale. The broadly used correction for the pD determination, pD ≈ $pH_{ms(D)}$ + 0.4 (where $pH_{ms(D)}$ refers to the pH-meter reading in D_2O solutions[78−81]) is due to intrinsic properties of the electrode's glass membrane.[116] Systematic studies on side-group pK_a shifts in D_2O[79,80] have demonstrated that the consistent comparison of proteins' charge states requires that parameters such as E_0 or k^0 should be compared under conditions of nearly equal pH-meter readings in H_2O and D_2O solutions; that is, virtually no correction to $pH_{ms(D)}$ is required.[79,80] Indeed, the KIE inversion almost disappears when the latter condition is applied (see the dotted curve in Figure 5b). In this context, the large inverse KIE for ET detected in ref 48 for freely diffusing Mb, obviously, cannot be explained by any error for the pD scaling. Rather, the rigidifying (stabilizing) impact of D_2O versus H_2O (see, e.g., refs 80 and 117) seems to cause an essential restriction of the conformational flexibility that blocks the ligating water's prolonged translocation, a situation resembling that for surface-confined (tightly bound) Mb in the present study (vide infra). The almost exponential change of the ET rate with the D_2O fraction in H_2O/D_2O mixed electrolyte solutions[48] confirms a version of the D_2O-induced triggering of the tight Mb conformation. Importantly, in the case of tight interfacial confinement, transfer into D_2O solution seemingly causes only minor additional conformational stabilization of Mb.

Furthermore, study of the impact of temperature and pressure effects normally provides valuable information on fine mechanistic details of biomolecular processes, including ET (see refs 4, 6, 20−26, 34−36, 39−42, 67−71, 86, 87, 95−99, and 110). Specifically, in a nonadiabatic regime of ET (eq 4), activation enthalpy, ΔH_a, can be directly judged against the reorganization Gibbs energy, λ_0 (through eqs 5 and 6),

dx.doi.org/10.1021/jp4101569 | J. Phys. Chem. B 2014, 118, 692−706

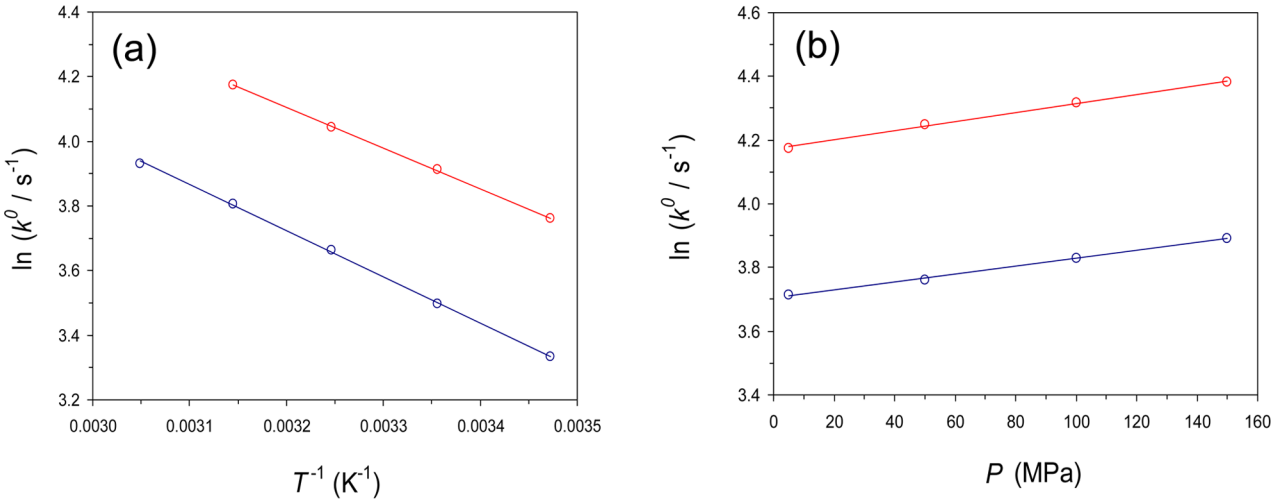

Figure 6. Dependencies of the standard rate constant for Mb electron exchange at Au/SAM junctions as a functions of (a) temperature (Arrhenius plots) and (b) pressure (semilogarithmic plots), in both H_2O and D_2O, pH (pD) 7.4 (Tris buffer), for the Mb sample that exhibited the maximum inverted KIE of 0.7 under standard conditions (25 °C, 0.1 MPa).

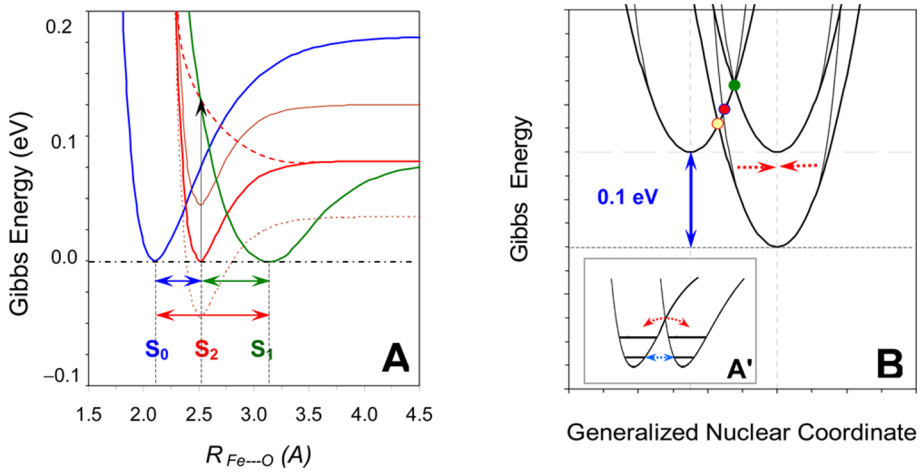

Figure 7. Schematic representation of free energy cross sections along (A) the heme−water (iron−oxygen) chemical bond formation (breakdown) coordinate, where R represents the Fe···O distance, and (B) the overall generalized reaction coordinate. Panel A depicts the energy curves attributable to S_0, S_2, and S_1, all of which are effectively bonding states.[62] The blue curve matches the singlet state of the ferric metmyoglobin, $MbFe^{3+}H_2O$, with the shortest Fe···O bond (~2.11 Å); the bold red curve matches the quintet state of the ferrous form, $MbFe^{2+}H_2O$, with the intermediate Fe···O bond (~2.49 Å), and the bold green curve matches the triplet state with the weakest Fe···O bond (~3.23 Å). The double-sided blue arrow shows the Fe···O bond reorganization during electron exchange in a tight complex. Panel A′ (inset of panel B) depicts this kind of transition, simultaneously showing the alternative, classical, and quantum patterns.[74] The vertical black arrow in panel A shows the first step of the reversible photodissociation process of water from $MbFe^{2+}H_2O$ below 100 K, observed in refs 21 and 22. A thermally activated equilibrium between these states shown by the double-sided green arrow has also been well-documented.[39−42] In both panels A and B the case of the zero energy gap, matching the standard rate constant of ET, along with the overvoltage variation are schematically shown. Panel B also shows the deviation of the shape of the energy curve from that of the harmonic curve, presumably leading to various deviations from the classical fitting pattern depicted in Figure 2a,b; see text for further details.

provided that the activation entropy is assumed to be negligible.[86,118,119] The Arrhenius-like plotting of $\ln(k^0)$ versus T^{-1} provides the activation enthalpy through the equation (see refs 4, 34, 68−71, 84−87, and 110)

$$\left[\frac{\partial(\ln k^0)}{\partial(1/T)}\right]_P = -\frac{\Delta H_a}{R} \quad (7)$$

Similarly, the dependence of $\ln(k^0_{ET})$ on P provides the activation volume, ΔV_a (whose value is also sensitive regarding the ET regime; see refs 82−87, 120, and 121), through the equation (see refs 6, 84−87, 110, and 120−124)

$$\left[\frac{\partial(\ln k^0)}{\partial P}\right]_T = -\frac{\Delta V_a}{RT} \quad (8)$$

Over limited ranges of T and P, these dependencies can be considered linear, and the corresponding values of the activation parameters can be considered as nearly constant (see Figure 6 and Table 1).

Figure 6 depicts the temperature (Arrhenius) and pressure dependencies of k^0 taken at pH 7.4 (Tris buffer), in both H_2O and D_2O, for the Mb sample that exhibited the maximum "inverted" KIE (see Figure 5b and Table 1 for the respective activation parameters and the discussion above). The obtained

dx.doi.org/10.1021/jp4101569 | J. Phys. Chem. B 2014, 118, 692−706

values of the activation parameters, ΔH_a and ΔV_a, are the same within the experimental error for H_2O and D_2O, indicating that these parameters might also be virtually independent of variable pH or pD (note the small absolute value of KIE throughout) and, hence, the method of comparison of k^0 in H_2O and D_2O. The values of ΔH_a are also in agreement with the value for λ_0, implying that the one-fourth rule is valid and that the activation entropy is negligible (that is, $\Delta H_a \approx \lambda_0/4$,[86,118,119] vide supra). The latter fact is in a good agreement with our conjecture that the resulting ET free energy surfaces, including the inner-sphere component depicted as the inset in Figure 7, implying classical barrier crossing along R, vide supra, have nearly parabolic (harmonic) shapes up to the point of the energy curve crossing (that is, the barrier top at zero energy gap). Indeed, according to Figure 2, deviations from the parabolic shape start to develop above the overvoltages of 0.10−0.15 V (10−15 kJ mol^{-1}). Furthermore, the obtained value for the activation volume is in agreement with those ascribed earlier to the nonadiabatic mechanism for long-range ET with cyt-c[83,110] and azurin.[86,87,110]

Atomistic Picture of ET-Coupled Water Displacement. The contemporary generalized (multidimensional) theory of charge transfer allows for a consideration of coupling of the outer-sphere ET (both long- and short-range) to different degrees of freedom of the medium, including the first ligand-sphere vibrational (quasiharmonic)[69,70,74−78] and associative/dissociative[125−127] modes, environmental (solvent-related, interfacial, and macromolecular) ballistic (see refs 67−70, 74, 76, and 104−107) and dissipative (see refs 100−103, 109, 110, and 128−130) modes, and so on. Examples of respective atomistic analysis of the ligand association/dissociation at model hemes[59−63] and in globins[59−61,64−66] and for ET (electron exchange) in "simple" iron hexaaqua complexes[74−78] are available. In this subsection, based on the principles of the generalized theoretical approach and in the spirit of the above-mentioned preceding work, we attempt to construct a combined model encompassing elementary processes, with the involvement of metmyoglin ($MbFe^{3+}H_2O$) and deoxymyoglobin ($MbFe^{2+}H_2O$; the associated, metastable and dissociated forms, respectively, vide infra), under diverse experimental conditions, including those of the present work. More specifically, these events are as follows:

(a) fast and reversible ET (electron exchange) between the electrode and metmyoglobin tightly immobilized through the appropriately designed SAMs ("simple docking", according to the terminology of refs 10 and 13−17), which is the present case and, presumably, the case of ET in a solution-phase "re-engineered" [Mb; cyt-b_5] complex;[14−17]

(b) low-temperature reduction of a "frozen" solution-phase metmyoglobin,[39−42] with the water molecule still bound to the reduced heme iron (the metastable state observed below 100 K; note that, under these experimental conditions, water dissociated from the heme at temperatures above 140 K[39−42]);

(c) simple reversible water photodissociation (and, hence, rebinding) from the reduced state of metmyoglobin below 100 K,[21,22] in which, presumably, water's translocation is restricted through the conformational constrains in solidified medium (see below);

(d) electrochemical quasireversible reduction of "freely diffusing" metmyoglobin, which is a very slow ET process, seemingly coupled to water dissociation/rebinding, which is, in turn, coupled to the "extra" reorganization of the water network within the ligand channel,[44−49] and related conformational rearrangements around the ligand entry site (gate opening).[34−43]

Figures 7A,B schematically depict free energy cross sections along the heme−water (iron−oxygen) chemical bond formation (breakdown) coordinate, with $R_{Fe\cdots O}$ representing the Fe···O distance, and the overall generalized reaction coordinate, respectively, with the latter enveloping all of the classical vibrational degrees of freedom subject to the ET-coupled reorganization. Figure 7A was mainly constructed according to the work of Strickland and Harvey,[62] in which, for the model system Fe/imidazol/porphyrin/water, three attractive Fe−OH_2 energy curves were identified, resembling the ferric singlet (S_0), ferrous triplet (S_1), and ferrous quartet (S_2) states. The latter two states, in essence, are nonbonding in nature; however, the repulsive three-electron versus two-center interaction, according to ref 62, is more than compensated by the larger electrostatic energy of attraction between the water dipole and the positive charge on the iron. In Figure 7A, the blue curve matches the singlet state of the ferric metmyoglobin, $MbFe^{3+}H_2O$, with the shortest Fe···O bond (∼2.11 Å) within the sequence; the bold red curve matches the quintet state of the ferrous form, $MbFe^{2+}H_2O$, with the intermediate Fe···O bond length (∼2.49 Å); and the bold green curve matches the triplet state with the weakest Fe···O bond (∼3.23 Å). The double-sided blue arrow shows the Fe···O bond reorganization during electron exchange in a tight complex (case a discussed above). This implies simple bond elongation/shortening coupled to a reversible ET, just as in the liquid-phase or interfacial ET processes involving the $[Fe(H_2O)_6]^{2+/3+}$ couple.[72−76] Indeed, calculations for simple $[Fe(H_2O)_5]^{3+/2+}$−OH_2 systems,[131,132] comparable to those by Strickland and Harvey[62] for a model Fe/imidazol/porphyrin/water system, showed remarkable qualitative similarities between respective spin states and the energy term sequence; yet, the quantitative difference is evident through the higher binding energies and corresponding shorter Fe···OH_2 bond distances for all of the spin states involved, for the case of hexaaquairon complexes. The previous theory-based analysis[74] demonstrated that, for the latter model system, around room temperature, thermally activated overbarrier (classical) surmounting prevails over the pure (zero-energy) tunneling pattern. However, at deeply cryogenic temperatures, the tunneling mechanism should become solely possible.[22] The inset in Figure 7B (denoted panel A′) depicts a transition along such a dualistic degree of freedom, simultaneously showing the alternative, classical, and quantum (that is, the nearly room-temperature and ultra-low-temperature) patterns (vide infra).

Figure 7B also shows deviation in the shape of the overall Gibbs energy curve from the harmonic one (due to the input from increasingly steepening conformational wells,[87,100−107] vide supra), presumably leading to various deviations from the Marcus-type standard fitting pattern, depicted in Figure 2a,b. In both panels A and B of Figure 7, the case of the zero energy gap that matches the standard situation in electrochemical science, yielding the standard rate constant of ET,[86−91,108−110] is shown as a main (starting) condition. In the original work by Strickland and Harvey,[62] both states S_2 and S_1 were found to lie higher in energy compared to S_0. However, one should note that, in that work, interaction of the model Fe/imidazol/

dx.doi.org/10.1021/jp4101569 | J. Phys. Chem. B 2014, 118, 692−706

porphyrin/water moiety with the protein environment was not taken into account. It has been demonstrated that this kind of interaction is able (and, actually, is organized such) to readily change the equilibrium between Mb's different spin states, thanks to the fine-tuning through the intraglobular hydrogen-bonding and/or long-range electrostatic interactions.[133−135] In turn, as mentioned above, the protein's structural and dynamic properties and, hence, the vertical disposition of the initial (reactant) and final (product), that is, the "channel", Gibbs energy terms can be readily tuned by the immediate environment (e.g., through the ligand-sphere and protein matrix arrangement), as well as through external perturbations (chemical modifications, physical confinement, electric field, etc.) (see refs 2−5, 34−56, 82−87, 110, 120, 121, 129, 130, 133, 136, and 137). Certainly, the shapes of the overall (multidimensional) and contributing Gibbs energy wells and their vertical dispositions are controlled by the variety of all these factors. According to one key result of fundamental theory,[69,126] at least approximately (depending on the deviations from the classical Marcus, i.e., perfectly harmonic, model), under the condition of $V_{AB} \ll RT$ (typical for the nonadiabatic ET regime, that is, the present case), in general, the slopes of the initial and final resulting Gibbs energy terms along all of the classical reaction coordinates (k = 1, ..., n), in the area of transition state ("saddle point") can be described by the equation

$$(1 - \alpha)\frac{\partial G_i}{\partial r_k} + \alpha\frac{\partial G_f}{\partial r_k} = 0 \tag{9}$$

where the subscripts i and f indicate initial and final resulting Gibbs energy slopes, respectively, along all of the classical reaction coordinates (k = 1, ..., n) in the area of saddle point and α is the transmission factor, defined as

$$\alpha = \frac{\partial(\Delta G_a)}{\partial(\Delta G_0)} = \frac{1}{2} + \frac{\Delta G_0}{2\lambda_0} \tag{10}$$

Equation 10 can be readily derived from eq 6, implying that the harmonic approximation is valid well above the energy curves' intersection point; see Figure 7 (i.e., at moderate overpotentials; not very distinct from the equilibrium potential, vide supra). It is convenient to consider the zero-overvoltage condition that corresponds to the zero free energy gap situation for the overall Gibbs energy terms (Figure 7B) as a basic (starting) condition, because for this state, eq 10 immediately results in α = 0.5, and eq 9 results in the expression

$$\frac{\partial G_i}{\partial r_k} = -\frac{\partial G_f}{\partial r_k} \tag{11}$$

The latter result indicates that, under this starting condition, the slopes of initial and final resulting Gibbs energy terms along all of the classical reaction coordinates in the area of saddle point are nearly equal. Consequently, the equilibrium potential for a given redox core is settled according to the system's ability to satisfy the condition of eq 9 with the participation of all classical degrees of freedom, including the outer-sphere and inner-sphere active (reorganizable) modes intrinsically coupled to ET. According to this picture, any deviation from the equilibrium potential (overpotential variation) leads to corresponding changes in the relative vertical alignment for the resulting Gibbs energy terms along the generalized reaction coordinate, as well as their cross sections along the individual variables.

The vertical black arrow in Figure 7A shows the first step of the reversible photodissociation process of water from $MbFe^{2+}H_2O$ below 100 K, observed by Nienhaus et al. in refs 21 and 22 (case c discussed above). A thermally activated equilibrium between these states shown by the double-sided green arrow has also been well-documented.[39−42] Interestingly, Nienhaus et al.[22] reported on the quantum-mechanical mechanistic pattern (H_2O tunneling) at cryogenic temperatures below 100 K and roughly estimated a tunneling distance of ca. 1 Å in the rebinding process of the displaced water. The distance between the S_2 and S_1 states (0.74 Å) found by Strickland and Harvey[62] approximately matches the tunneling distance estimated on the basis of cryogenic kinetic experiments of Nienhaus et al.[22] Importantly, for the deoxy structure of sperm whale Mb at room temperature, the X-ray data of Parak et al.[40] revealed a site inside the distal pocket that is 3.6 Å from the iron. If one assumes that the protein environment, including the hydrogen bonding of a ligand water with the His-64 imidazole, along with the energy stabilization of the S_1 state, also alters its respective energy minimum position to set the Fe···OH_2 distance at 3.6 Å (compared to that found for the model porphyrine system by Strickland and Harvey[62]), the low-temperature tunneling distance between the S_2 and S_1 states (assuming much less influence of protein on the S_2 state) now would appear to be ca. 1.1 Å, that is, perfectly matches with the value deduced from the cryogenic kinetic experiments of ref 22. The latest, most sophisticated MD calculations offered adiabatic energy cross sections for some heme−ligand binding reaction coordinates, indicating the existence of the extra energy minimum at larger Fe···ligand separations (for CO and NO, but not for H_2O) resembling the so-called remote Xe4 site.[65,66] We set the question open for further detailed studies whether the excitation in mechanism c considered above leads to water's direct or stepwise photodissociation into the site detected by Parak et al.[40] or the Xe4 site (followed by an eventual dropping into the "pre-final" S_1 state), through the completely repulsive energy term or through direct optical transfer to this temporary state. Actually, both scenarios (parallel reaction channels) might be realized simultaneously. At any rate, the electrochemical electron exchange for a freely diffusing, very loosely confined Mb (case d listed above), which seems to be highly inefficient in ET, can hardly be coupled to the complete dissociation/association of the ligand water. The reverse (oxidation) voltammetric peaks normally cannot be observed for the case of dissociative ET.[127] We suppose that, for the case of free Mb, its internal flexibility allows for the ET pattern coupled to a larger, yet still reversible water displacement from S_0 directly to the S_1 state, which, under another distinct conformational condition, might become better available for coupling to ET. The position shift of the water molecule in case d in Figure 7A is shown by the double-sided red arrow. The overall reorganization Gibbs energy for the latter case has been proposed to exceed that in case a of the present study (by the simple comparison of standard rate constants) by ca. 0.2 eV.[48]

Special attention should be paid to the question of electronic coupling between the initial and final states of a rather complex process under the main focus of this article, encompassing both the long-range outer-sphere ET (which is traditionally sketched as Figure 7B) and inner-sphere reorganization of the water ligand accompanied by a corresponding change of iron's spin state (between the S_0 and S_2 states, here originally depicted in Figure 7A). Spin inversion processes, in general, are deemed to be formally forbidden and, hence, very slow, because of very

dx.doi.org/10.1021/jp4101569 | J. Phys. Chem. B 2014, 118, 692−706

low electronic coupling between the reactant and product states.[138] Yet, it has been proposed that, in globins, thanks to the protein's spin-tuning properties, the values of V_{AB} for ligand binding/release are much higher than those for model porphyrin systems.[139] However, for electrochemical devices such as ours, there is another serious reason for the lowering of the V_{AB} value. According to the general theory,[68−71] the overall energy splitting (value of V_{AB} in eq 4) is identical along all of its cross sections for all the contributing classically behaved degrees of freedom (reaction coordinates) and is set collectively by the system's electronic subsystem. For cases in which outer-sphere ET additionally is involved, the value of V_{AB} decays exponentially with the outer-sphere ET distance, R_{ET}, according to the equation (see refs 83−86, 90−93, 108−110, 118, 119, and 140)

$$V_{AB} = V^0_{AB} \exp[-\beta(R_{ET} - R^0_{ET})] \quad (12)$$

in which V^0_{AB} is the electronic coupling at the hypothetically closest possible approach between electron-donor and -acceptor species, R^0_{ET} (usually considered as a van der Waals distance between the reactants' metal cores); in our system, R_{ET} represents the actual distance between an electrode surface and the heme iron core, amounting to ca. 20 Å, with a large contribution from the SAM thickness of ca. 15 Å (see refs 109, 110, and 140) and β is the decay coefficient, which has a value of ca. 1 $Å^{-1}$ for alkanethiol SAMs (see refs 83−86, 90−93, 108−110, 118, and 119). Based on these theoretical notions and existing literature data, one can propose an approximate value for V_{AB} of ca. 10^{-6} eV for our system, provided that the contribution from the iron spin-inversion component is not a bottleneck. The comparative analysis of the present kinetic data for Mb and matching literature data for cyt-*c* under comparable ET condition (Figure 4 and Table 1) indicates that the contribution to V_{AB} from the spin-state changeover for Mb is comparable to that for cyt-*c*. Hence, in both cases, very similar values for V_{AB} and reorganization Gibbs energies (both inner- and outer-sphere) are expected.

SUMMARY

Extremely tight immobilization of horse muscle Mb at a Au-deposited 1:1 mixed $HS-(CH_2)_{11}-COOH/HS-(CH_2)_{11}-OH$ SAM has been achieved. The clear voltammetric (CV) response was highly stable and reproducible even after repetitive temperature and pressure cycling over the ranges of 15−55 °C and 0.01−150 MPa, respectively.

The value of the rate constant for the electron exchange with the Au electrode through SAMs of variable composition but virtually same thickness was found to correlate positively with the strength of the Mb immobilization as judged by the CV signal stability.

Whereas the voltammetric signal, at relatively low scan rates (i.e., before the overvoltage of 0.10−0.15 was reached), was very stable (robust) and followed the trend set by the Marcus model (validating reliable determination of the sought kinetic parameters), above this threshold, it displayed specific instability (variability) regarding different factors such as date of sample issue, simple aging for several hours, pH, and pressure and temperature cycling.

The observed deviations from the Marcus pattern can be explained by the involvement of the conformational component in the resulting ET free energy surface tending to deviate from the parabolic shape at their energy values exceeding 0.10−0.15 eV (nearly above the curve crossing under the zero-overvoltage condition).

The pH-dependent inverted small KIE turned apparently normal when the actual charged states of the Mb molecule were taken into the account, which can be explained through the minor involvement of proton translocations belonging to remote ionizable (imidazole) groups of Mb.

The whole variety of our experimental data, at the atomistic level, can be explained on the basis of contemporary generalized (multidimensional) ET theory, implying that strong immobilization (tight docking) leads to the restricted environmental configuration, allowing the reversible ET process to be coupled to a minor inner-sphere reorganization (elongation/shortening of an $Fe-OH_2$ bond) rather than to the pronounced detachment (rebinding) of water.

In contrast, physiological full water release from deoxy-Mb probably occurs by way of a cooperative translocation through the whole hydrogen-bonded water chain inside the ligand channel. In the first, ET-coupled elementary stage, water can be displaced from the heme iron significantly (from S_0 to S_1). The corresponding free energy of reorganization should be large and may slow the ET process significantly. This actually takes place in a natural, loosely bound precursor complex with cyt-b_5, also allowing for water replacement by the key ligand, O_2, through the still-accessible ligand channel.

AUTHOR INFORMATION

Corresponding Authors

*E-mail: dimitri.khoshtariya@tsu.ge.

*E-mail: vaneldik@chemie.uni-erlangen.de.

Notes

The authors declare no competing financial interest.

ACKNOWLEDGMENTS

Research grants from the Volkswagen Foundation, Hannover, Germany, I/83-395 and I/85-642 (R.v.E., D.E.K., T.D.D., M.S.); Rustaveli National Science Foundation, Tbilisi, Georgia, GNSF/ST08/2-374 and FR/771/7-230/11 (D.E.K., T.D.D., M.S.); and the Deutsche Forschungsgemeinschaft (DFG), Bonn, Germany, as part of SFB-583 on "Redox-Active Metal Complexes" (R.v.E.) are gratefully acknowledged. D.E.K acknowledges senior fellowships from the Alexander von Humboldt Foundation, Bonn, Germany (2010, 2013). T.D.D. acknowledges a senior fellowship from the Deutsche Akademische Austauschdienst (DAAD), Bonn, Germany (2011).

REFERENCES

(1) Antonioni, E.; Brunori, M. *Hemoglobin and Myoglobin in their Reactions with Ligands*; North-Holland: Amsterdam, 1971.

(2) Parak, F. G.; Nienhaus, G. U. Myoglobin, a Paradigm in the Study of Protein Dynamics. *Chem. Phys. Chem.* **2002**, *3*, 249−254.

(3) Frauenfelder, H.; McMahon, B. H.; Fenimore, P. W. Myoglobin: The Hydrogen Atom of Biology and a Paradigm of Complexity. *Proc. Natl. Acad. Sci. U.S.A.* **2003**, *100*, 8615−8617.

(4) Frauenfelder, H.; Chen, G.; Berendzen, J.; Fenimore, P. W.; Jansson, H.; McMahon, B. H.; Stroe, I. R.; Swenson, J.; Young, R. D. A Unified Model of Protein Dynamics. *Proc. Natl. Acad. Sci. U.S.A.* **2009**, *106*, 5129−5134.

(5) Brunori, M. Myoglobin Strikes Back. *Protein Sci.* **2010**, *19*, 195−201.

(6) Brindell, M.; Stawoska, I.; Orzeł, L.; Labuz, P.; Stochel, G.; van Eldik, R. Application of High Pressure Laser Flash Photolysis in

Studies on Selected Hemoprotein Reactions. *Biochim. Biophys. Acta* **2008**, *1784*, 1481−1492.
(7) Kiger, L.; Tilleman, L.; Geuens, E.; Hoogewijs, D.; Lechauve, C.; Moens, L.; Dewilde, S.; Marden, M. C. Electron Transfer Function versus Oxygen Delivery: A Comparative Study for Several Hexacoordinated Globins Across the Animal Kingdom. *PLOS One* **2011**, *6*, e20478 (10).
(8) Hagler, L.; Coppes, R. I.; Herman, R. H. Metmyoglobin Reductase. *J. Biol. Chem.* **1979**, *254*, 6505−6514.
(9) Beckit, A. E. D.; Faustman, C. Metmyoglobin Reducing Activity. *Meat Sci.* **2005**, *71*, 407−439.
(10) Cowan, J. A.; Upmacis, R. K.; Beratan, D. N.; Onuchic, J. N.; Gray, H. B. Long-Range Electron Transfer in Myoglobin. *Ann. N.Y. Acad. Sci.* **1988**, *550*, 68−84.
(11) Battistuzzi, G.; Bellei, M.; Casella, L.; Bortolotti, C. A..; Roncone, R.; Monzani, E.; Sola, M. Redox Reactivity of Heme Fe^{3+}/Fe^{2+} Couple in Native Myoglobins and Mutants with Peroxidase-like Activity. *J. Biol. Inorg. Chem.* **2007**, *12*, 951−958.
(12) D'Antonio, E. L.; D'Antonio, J.; de Serrano, V.; Gracz, H.; Thompson, M. K.; Ghiladi, R. A.; Bowden, E. F.; Franzen, S. Functional Consequences of the Creation of an Asp-His-Fe Triad in a 3/3 Globin. *Biochemistry* **2011**, *50*, 9664−9680.
(13) Liang, Z.-X.; Kurnikov, I. V.; Nocek, J. M.; Mauk, A. G.; Beratan, D. N.; Hoffman, B. M. Dynamic Docking and Electron Transfer between Cytochrome b_5 and Suite of Myoglobin Surface-Charge Mutants. Introduction of a Functional-Docking Algorithm for Protein−Protein Complexes. *J. Am. Chem. Soc.* **2004**, *126*, 2785−2798.
(14) Wheeler, K. E.; Nocek, J. M.; Cull, D. A.; Yatsunyk, L. A.; Rosenzweig, A. C.; Hoffman, B. M. Dynamic Docking of Cytochrome b_5 with Myoglobin and α-Hemoglobin: Heme-Neutralization "Squares" and the Binding of Electron-Transfer-Reactive Configurations. *J. Am. Chem. Soc.* **2007**, *129*, 3906−3917.
(15) Xiong, P.; Nocek, J. M.; Griffin, A. K. K.; Wang, J.; Hoffman, B. M. Electrostatic Redesign of the [Myoglobin, Cytochrome b_5] Interface To Create a Well-Defined Docked Complex with Rapid Interprotein Electron Transfer. *J. Am. Chem. Soc.* **2009**, *131*, 6938−6939.
(16) Xiong, P.; Nocek, J. M.; Vura-Weis, J.; Lockard, J. V.; Wasielewski, M. R.; Hoffman, B. M. Faster Interprotein Electron Transfer in a [Myoglobin, b5] Complex with a Redesigned Interface. *Science* **2010**, *330*, 1075−1078.
(17) Nocek, J. M.; Knutson, A. K.; Xiong, P.; Petlakh Co, N.; Hoffman, B. M. Photoinitiated Singlet and Triplet Electron Transfer across a Redesigned [Myoglobin, Cytochrome b_5] Interface. *J. Am. Chem. Soc.* **2010**, *132*, 6165−6175.
(18) Peisach, J.; Mims, W. B.; Davis, J. L. Water Coordination by Heme Iron in Metmyoglobin. *J. Biol. Chem.* **1984**, *259*, 2704−2706.
(19) Rajarathnam, K.; La Mar, G. N.; Chiu, M. L.; Sligar, S. G.; Singh, J. P.; Smith, K. M. ^{1}H NMR Hyperfine Shift Pattern as a Probe for Ligation State in High-Spin Ferric Hemoproteins: Water Binding in Metmyoglobin Mutants. *J. Am. Chem. Soc.* **1991**, *113*, 7886−7892.
(20) Cao, W.; Christian, J. F.; Champion, P. M.; Rosca, F.; Sage, J. T. Water Penetration and Binding to Ferric Myoglobin. *Biochemistry* **2001**, *40*, 5728−5737.
(21) Lamb, D. C.; Prusakov, V. E.; Engler, N.; Ostermann, A.; Schellenberg, P.; Parak, F. G.; Nienhaus, G. U. Photodissociation and Rebinding of H_2O to Ferrous Sperm Whale Myoglobin. *J. Am. Chem. Soc.* **1998**, *120*, 2981−2982.
(22) Lamb, D. C.; Kriegl, J.; Kastens, K.; Nienhaus, G. U. Quantum-Mechanical Tunneling of Water in Heme Proteins. *J. Phys. Org. Chem.* **2000**, *13*, 659−663 2000.
(23) Ouellet, Y. H.; Daigle, R.; Lagu, P.; Dantsker, D.; Milani, M.; Bolognesi, M.; Friedman, J. M.; Guertin, M. Ligand Binding to Truncated Hemoglobin N from *Mycobacterium tuberculosis* Is Strongly Modulated by the Interplay between the Distal Heme Pocket Residues and Internal Water. *J. Biol. Chem.* **2008**, *283*, 27270−27278.
(24) Goldbeck, R. A.; Bhaskaran, S.; Ortega, C.; Mendoza, J. L.; Olson, J. S.; Soman, J.; Kliger, D. S.; Esquerra, R. M. Water and Ligand Entry in Myoglobin: Assessing the Speed and Extent of Heme Pocket Hydration after CO Photodissociation. *Proc. Natl. Acad. Sci. U.S.A.* **2006**, *103*, 1254−1259.
(25) Esquerra, R. M.; Jensen, R. A.; Bkhaskaran, S.; Pillbury, M. L.; Mendosa, J. L.; Lintner, B. W.; Kliger, D. S.; Goldbeck, R. A. The pH Dependence of Heme Pocket Hydration and Ligand Rebinding Kinetics in Photodissociated Carbonmonoxymyoglobin. *J. Biol. Chem.* **2008**, *283*, 14165−14175.
(26) Esquerra, R. M.; Lopez-Pena, I.; Tipgunlakant, P.; Birukou, I.; Nguen, R. L.; Soman, J.; Olson, J. S; Kliger, D. S.; Goldbeck, R. A. Kinetic Spectroscopy of Heme Hydration and Ligand Binding in Myoglobin and isolated Hemoglobin Chains: An Optical Window into Heme Pocket Water Dynamics. *Phys. Chem. Chem. Phys.* **2010**, *12*, 10270−10278.
(27) Quillin, M. L.; Arduni, R. M.; Olson, J. S.; Phillips, G. N. High-Resolution Crystal Structures of Distal Histidine Mutants of Sperm Whale Myoglobin. *J. Mol. Biol.* **1993**, *234*, 140−155.
(28) Yang, F.; Phillips, G. N. Crystal Structures of CO-, Deoxy-, and Met-Myoglobins at Various pH values. *J. Mol. Biol.* **1996**, *256*, 762−774.
(29) Schote, F.; Soman, J.; Olson, J. S.; Wulff, M.; Anfinrud, P. A. Picosecond Time-Resolved X-ray Crystallography: Probing Protein Function in Real Time. *J. Struct. Biol.* **2004**, *147*, 235−246.
(30) Bourgeois, D.; Vallone, B.; Arcovito, A.; Sciara, G.; Schotte, F.; Anfinrud, P. A.; Brunori, M. Extended Subnanosecond Structural Dynamics of Myoglobin Revealed by Laue Crystallography. *Proc. Natl. Acad. Sci. U.S.A.* **2006**, *103*, 4924−4929.
(31) Schotte, F.; Sun Cho, H.; Soman, J.; Wulff, M.; Olson, J. S.; Anfinrud, P. A. Real-Time Tracking of CO Migration and Binding in the α and β Subunits of Human Hemoglobin via 150-ps Time-Resolved Laue Crystallography. *Chem. Phys.* **2013**, *422*, 98−106.
(32) Cocco, M. J.; Kao, Y.-H.; Philips, A. T.; Lecomte, J. T. J. Structural Comparison of Apomyoglobin and Metaquomyoglobin: pH Titration of Hystidines by NMR Spectroscopy. *Biochemistry* **1992**, *31*, 6481−6491.
(33) Svistunenko, D. A.; Sharpe, M. A.; Nicholls, P.; Blenkinsop, C.; Davies, N. A.; Dunne, J.; Wilson, M. T.; Cooper, C. E. The pH Dependence of Naturally Occurring Low-Spin Forms of Methaemoglobin and Metmyoglobin: An EPR Study. *Biochem. J.* **2000**, *351*, 595−605.
(34) Steinbach, P. J.; Ansari, A.; Berendzen, J.; Braunstein, D.; Chu, K.; Cowen, B. R.; Ehrenstein, D.; Frauenfelder, H.; Johnson, B. J. Ligand Binding to Heme Proteins: Connection between Dynamics and Function. *Biochemistry* **1991**, *30*, 3988−4001.
(35) Tian, W. D.; Sage, J. T.; Champion, P. M. Investigation of Ligand Association and Dissociation Rates in the "Open" and "Closed" States of Myoglobin. *J. Mol. Biol.* **1993**, *233*, 155−166.
(36) Dantsker, D.; Samuni, U.; Friedman, J. M.; Agmon, N. A Hierarchy of Functionally Important Relaxations within Myoglobin Based on Solvent Effects, Mutations and Kinetic Model. *Biochim. Biophys. Acta* **2005**, *1749*, 234−251.
(37) Nishihara, Y.; Kato, S.; Hayashi, S. Protein Collective Motions Coupled to Ligand Migration in Myoglobin. *Biophys. J.* **2010**, *98*, 1649−1657.
(38) Scorciapino, M. A.; Robertazzi, A.; Casu, M.; Ruggerone, P.; Ceccarelli, M. Heme Proteins: The Role of Solvent in the Dynamics of Gates and Portals. *J. Am. Chem. Soc.* **2010**, *132*, 5156−5163.
(39) Prusakov, V. E.; Steyer, J.; Parak, F. G. Mössbauer Spectroscopy on Nonequilibrium States of Myoglobin: A Study of r-t Relaxation. *Biophys. J.* **1995**, *68*, 2524−2530.
(40) Lamb, D. C.; Ostermann, A.; Prusakov, V. E.; Parak, F. G. From Metmyoglobin to Deoxy Myoglobin: Relaxations of an Intermediate State. *Eur. Biophys. J.* **1998**, *27*, 113−125.
(41) Engler, N.; Ostermann, A.; Gassmann, A.; Lamb, D. C.; Prusakov, V. E.; Schott, J.; Schweitzer-Stenner, R.; Parak, F. G. Protein Dynamics in an Intermediate State of Myoglobin: Optical Absorption, Resonance Raman Spectroscopy, and X-ray Structure Analysis. *Biophys. J.* **2000**, *78*, 2081−2092.
(42) Engler, N.; Prusakov, V. E.; Ostermann, A.; Parak, F. G. A Water Network within a Protein: Temperature-Dependent Water Ligation in

H64V-Metmyoglobin and Relaxation to Deoxymyoglobin. *Eur. Biophys. J.* **2003**, *31*, 595−607.
(43) King, B. C.; Hawkridge, F. M.; Hoffman, B. M. Electrochemical Studies of Cyanometmyoglobin and Metmyoglobin: Implications for Long-Range Electron Transfer in Proteins. *J. Am. Chem. Soc.* **1992**, *114*, 10603−10608.
(44) Van Dyke, B. R.; Saltman, P.; Armstrong, F. A. Control of Myoglobin Electron-Transfer Rates by the Distal (Nonbound) Histidine Residue. *J. Am. Chem. Soc.* **1996**, *118*, 3490−3492.
(45) Mie, Y.; Sonoda, K.; Neya, S.; Funasaki, N.; Taniguchi, I. Electrochemistry of Myoglobins Reconstituted with Azahemes and Mesohemes. *Bioelectrochem. Bioenerg.* **1998**, *46*, 175−184.
(46) Cohen, D. J.; King, B. C.; Hawkridge, F. M. Spectroelectrochemical and Electrochemical Determination of Ligand Binding and Electron Transfer Properties of Myoglobin, Cyanomyoglobin, and Imidazolemyoglobin. *J. Electroanal. Chem.* **1998**, *447*, 53−62.
(47) Duah-Williams, L.; Hawkridge, F. M. The Temperature Dependence of the Kinetics of Cyanide Dissociation from the Cyanide Complex of Myoglobin Studied by Cyclic Voltammetry. *J. Electroanal. Chem.* **1999**, *466*, 177−186.
(48) Mie, Y.; Yamada, C.; Uno, T.; Neya, S.; Mizutani, F.; Nishiyama, K.; Taniguchi, I. Notable Deuterium Effect on the Electron Transfer Rate of Myoglobin. *Chem. Commun.* **2005**, 250−252.
(49) Mie, Y.; Kishita, M.; Nishiyama, K.; Taniguchi, I. Interfacial Electron Transfer Kinetics of Myoglobins Chemically Modified with Succinic Anhydride at an Indium Oxide Electrode. *J. Electroanal. Chem.* **2008**, *624*, 305−309.
(50) Nassar, A.-E. F.; Zhang, Z.; Hu, N.; Rusling, J. F.; Kumosinski, T. F. Proton-Coupled Electron Transfer from Electrodes to Myoglobin in Ordered Biomembrane-Like Films. *J. Phys. Chem. B* **1997**, *101*, 2224−2231.
(51) Hu, N.; Rusling, J. F. Electrochemistry and Catalysis with Myoglobin in Hydrated Poly(ester sulfonic acid) Ionomer Films. *Langmuir* **1997**, *13*, 4119−4125.
(52) Feng, M.; Tachikawa, H. Raman Spectroscopic and Electrochemical Characterization of Myoglobin Thin Film: Implication of the Role of Histidine 64 for Fast Heterogeneous Electron Transfer. *J. Am. Chem. Soc.* **2001**, *123*, 3013−3020.
(53) Li, N.; Xu, J.-Z.; Yao, H.; Zhu, J.-J.; Chen, H.-Y. The Direct Electron Transfer of Myoglobin Based on the Electron Tunneling in Proteins. *J. Phys. Chem. B* **2006**, *110*, 11561−11565.
(54) Guo, c.; Sun, H.; Zhao, X. S. Myoglobin within Graphene Oxide Sheets and Nafion Composite Films as Highly Sensitive Biosensor. *Sens. Actuators B* **2012**, *164*, 82−89.
(55) D'Antonio, E. L.; Chen, T. K.; Turner, A. H.; Santiago-Capeles, L.; Bowden, E. F. Voltammetry of Dehaloperoxidase on Self-Assembled Monolayers: Reversible Adsorptive Immobilization of a Globin. *Electrochem. Commun.* **2013**, *26*, 67−70.
(56) Chen, T. K.; Bowden, E. F. Electrochemical Characterization of Dehaloperoxidase Adsorbates on COOH/OH Mixed Self-Assembled Monolayers. *J. Electroanal. Chem.* **2013**, *703*, 23−28.
(57) D'Antonio, J.; D'Antonio, E. L.; Thompson, M. K.; Bowden, E. F.; Franzen, S.; Smirnova, T.; Ghiladi, R. A. Spectroscopic and Mechanistic Investigations of Dehaloperoxidase B from *Amphitrite ornata*. *Biochemistry* **2010**, *49*, 6600−6616.
(58) Dolidze, T. D.; Khoshtariya, D. E.; van Eldik, R. Myoglobin at Au/SAM Junctions: Temperature, High Pressure and Solvent Kinetic Isotope Effects. *Eur. Biophys. J.* **2011**, *40* (S), 181 (P-541).
(59) Frauenfelder, H.; Wolynes, P. G. Rate Theories and Puzzles of Hemoprotein Kinetics. *Science* **1985**, *229*, 337−345.
(60) Šrajer, V.; Reinisch, L.; Champion, P. M.. Protein Fluctuations, Distributed Coupling, and the Binding of Ligands to Heme Proteins. *J. Am. Chem. Soc.* **1988**, *110*, 6656−6670.
(61) Zhu, L.; Sage, T.; Champion, P. M. Observation of Coherent Reaction Dynamics in Heme Proteins. *Science* **1994**, *266*, 629−632.
(62) Strickland, N.; Harvey, J. N. Spin-Forbidden Ligand Binding to the Ferrous−Heme Group: Ab Initio and DFT Studies. *J. Phys. Chem. B* **2007**, *111*, 841−852.
(63) Röhrig, U.; Grosdidier, A.; Zoete, V.; Michielin, O. Docking to Heme Proteins. *J. Comput. Chem.* **2009**, *30*, 2305−2315.
(64) Meuwly, M.; Becker, O. M.; Stote, R.; Karplus, M. NO rebinding to Myoglobin: A Reactive Molecular Dynamics Study. *Biophys. Chem.* **2002**, *98*, 183−207.
(65) Banushkina, P.; Meuwly, M. Free-Energy Barriers in MbCO Rebinding. *J. Phys. Chem. B* **2005**, *109*, 16911−16917.
(66) Nutt, D. R.; Meuwly, M. Studying Reactive Processes with Classical Dynamics: Rebinding Dynamics in MbNO. *Biophys. J.* **2006**, *90*, 1191−1201.
(67) Marcus, R. A. On the Theory of Electron-Transfer Reactions. VI. Unified Treatment for Homogeneous and Electrode Reactions. *J. Chem. Phys.* **1965**, *43*, 679−701.
(68) Dogonadze, R. R.; Kuznetsov, A. M. Theory of Charge Transfer Kinetics at Solid−Polar Liquid Interfaces. *Prog. Surf. Sci.* **1975**, *6*, 11−41.
(69) Dogonadze, R. R.; Kuznetsov, A. M.; Marsagishvili, T. A. The Present State of the Theory of Charge Transfer Processes in Condenced Phase. *Electrochim. Acta* **1980**, *25*, 1−28.
(70) Marcus, R. A.; Sutin, N. Electron Transfers in Chemistry and Biology. *Biochim. Biophys. Acta* **1985**, *811*, 265−322.
(71) Kuznetsov, A. M.; Ulstrup, J. *Electron Transfer in Chemistry and Biology*; Wiley: Chichester, U.K., 1999.
(72) Brunschwig, B. S.; Logan, J.; Newton, M. D.; Sutin, N. A Semiclassical Treatment of Electron-Exchange Reactions. Application to the Hexaaquoiron(II)−Hexaaquoiron(III) System. *J. Am. Chem. Soc.* **1980**, *102*, 5798−5809.
(73) Brunschwig, B. S.; Creutz, C.; Macartney, D. H.; Sham, T.-K.; Sutin, N. The Role of Inner-Sphere Configuration Changes in Electron-Exchange Reactions of Metal Complexes. *Faraday Discuss. Chem. Soc.* **1982**, *74*, 113−127.
(74) Kuharski, R. A.; Bader, J. S.; Chandler, D.; Sprik, M.; Klein, M. L.; Impey, R. W. Molecular Model for Aqueous Ferrous−Ferric Electron Transfer. *J. Chem.. Phys.* **1988**, *89*, 3248−3257.
(75) Zhang, D.; Liu, C. Reorganization Criteria and their Effects in Inner-Sphere Barriers for Transition Metal Redox Pairs $M(H_2O)_6^{2+/3+}$ (M = V, Cr, Mn, Fe and Co). *New J. Chem.* **2002**, *26*, 361−366.
(76) Drechsel-Grau, C.; Sprik, M. Activation Energy for a Model Ferrous−Ferric Half Reaction from Transition Path Sampling. *J. Chem. Phys.* **2012**, *136*, 034506 (11).
(77) Neumann, R. C.; Kauzmann, W.; Zipp, A. Pressure Dependence of Weak Acid Ionization in Aqueous Buffers. *J. Phys. Chem.* **1973**, *77*, 2687−2691.
(78) Covington, A. K.; Paabo, M.; Robinson, R. A.; Bates, R. G. Use of the Glass Electrode in Deuterium Oxide and the Relation between the Standardized pD (pa_D) Scale and the Operational pH in Heavy Water. *Anal. Chem.* **1968**, *40*, 700−706.
(79) Kalinichenko, L. P.; Lobyshev, V. I. Should the pH−pD Condition be Used in Biological Experiments with Heavy Water as a Solvent? *Stud. Biophys.* **1976**, *58*, 235−240.
(80) Lobyshev, V. I.; Kalinichenko, L. P. *Isotope Effects of D_2O in Biological Systems*; Nauka: Moscow, U.S.S.R., 1978 (in Russian).
(81) Krezel, A.; Bal, W. A Formula for Correlating pKa Values Determined in D_2O and H_2O. *J. Inorg. Biochem.* **2004**, *98*, 161−166.
(82) Dolidze, T. D.; Khoshtariya, D. E.; Waldeck, D. H.; Macyk, J.; van Eldik, R. Positive Activation Volume for a Cytochrome C Electrode Process: Evidence for a "Protein Friction" Mechanism from High-Pressure Studies. *J. Phys. Chem. B* **2003**, *107*, 7172−7179.
(83) Khoshtariya, D. E.; Dolidze, T. D.; Seifert, S.; Sarauli, D.; Lee, G.; van Eldik, R. Kinetic, Thermodynamic, and Mechanistic Patterns for Free (Unbound) Cytochrome *c* at Au/SAM Junctions: Impact of Electronic Coupling, Hydrostatic Pressure, and Stabilizing/Denaturing Additives. *Chem.—Eur. J.* **2006**, *12*, 7041−7056.
(84) Dolidze, T. D.; Khoshtariya, D. E.; Illner, P.; Kulisiewicz, L.; Delgado, A.; van Eldik, R. High-Pressure Testing of Heterogeneous Charge Transfer in a Room-Temperature Ionic Liquid. Evidence for Solvent Dynamic Control. *J. Phys. Chem. B* **2008**, *112*, 3085−3100.
(85) Khoshtariya, D. E.; Dolidze, T. D.; van Eldik, R. Multiple Mechanisms for Electron Transfer at Metal/Self-Assembled Mono-

layer/Room-Temperature Ionic Liquid Junctions: Dynamical Arrest versus Frictional Control and Non-Adiabaticity. *Chem.—Eur. J.* **2009**, *15*, 5254−5262.
(86) Khoshtariya, D. E.; Dolidze, T. D.; Shushanyan, M.; Davis, K.; Waldeck, D. H.; van Eldik, R. Fundamental Signatures of Short- and Long-Range Electron Transfer for the Blue Copper Protein Azurin at Au/SAM Junctions. *Proc. Natl. Acad. Sci. U.S.A.* **2010**, *107*, 2757−2762.
(87) Khoshtariya, D. E.; Dolidze, T. D.; Tretyakova, T.; Waldeck, D. H.; van Eldik, R. Electron Transfer with Azurin at Au/SAM Junctions in Contact with a Protic Ionic Melt: Impact of Glassy Dynamics. *Phys. Chem. Chem. Phys.* **2013**, *15*, 16515−16526.
(88) Weber, K.; Creager, S. E. Voltammetry of Redox-Active Groups Irreversibly Adsorbed onto Electrodes. Treatment Using the Marcus Relation between Rate and Overpotential. *Anal. Chem.* **1994**, *66*, 3164−3172.
(89) Tender, L.; Carter, M. T; Murrey, R. W. Cyclic Voltammetric Analysis of Ferrocene Alkanethiol Monolayer Electrode Kinetics Based on Marcus Theory. *Anal. Chem.* **1994**, *66*, 3173−3181.
(90) Weber, K.; Hockett, L.; Creager, S. E. Long-Range Electronic Coupling between Ferrocene and Gold in Alkanethiolate-Based Monolayers on Electrodes. *J. Phys. Chem. B* **1997**, *101*, 8286−8291.
(91) Napper, A. M.; Liu, H.; Waldeck, D. H. The Nature of Electronic Coupling between Ferrocene and Gold through Alkanethiolate Monolayers on Electrodes: The Importance of Chain Composition, Interchain Coupling, and Quantum Interference. *J. Phys. Chem. B* **2001**, *105*, 7699−770.
(92) Yue, H.; Khoshtariya, D. E.; Waldeck, D. H.; Grochol, J.; Hildebrandt, P.; Murgida, D. H. On the Electron Transfer Mechanism between Cytochrome *c* and Metal Electrodes at Short Distances. Evidence for Dynamic Control. *J. Phys. Chem. B* **2006**, *110*, 19906−19913.
(93) Dolidze, T. D.; Rondinini, S.; Vertova, A.; Waldeck, D. H.; Khoshtariya, D. E. Impact of Self-Assembly Composition on the Alternate Interfacial Electron Transfer for Electrostatically Immobilized Cytochrome *c*. *Biopolymers* **2007**, *87*, 68−73.
(94) Fleming, B. D.; Praporski, S.; Bond, A. M.; Martin, L. L. Electrochemical Quartz Crystal Microbalance Study of Azurin Adsorbtion onto an Alkanethiol Self-Assambled Monolayer of Gold. *Langmuir* **2008**, *24*, 323−327.
(95) Zusman, L. D. Outer-Sphere Electron Transfer at an Electrode. *Chem. Phys.* **1987**, *112*, 53−59.
(96) Morgan, J. D.; Wolynes, P. G. Adiabaticity of Electron Transfer at an Electrode. *J. Phys. Chem.* **1987**, *91*, 874−883.
(97) Sumi, H.; Marcus, R. A. Dynamical Effects in Electron Transfer Reactions. *J. Chem. Phys.* **1986**, *84*, 4894−4914.
(98) Rips, I.; Jortner, J. Dynamic Solvent Effects on Outer-Sphere Electron Transfer. *J. Chem. Phys.* **1987**, *87*, 2090−2104.
(99) Mishra, A K.; Waldeck, D. H. A Unified Model for the Electrochemical Rate Constant that Incorporates Solvent Dynamics. *J. Phys. Chem. C* **2009**, *113*, 17904−17914.
(100) Miyashita, O.; Onuchic, J. N.; Wolynes, P. G. Nonlinear Elasticity, Proteinquakes, and the Energy Landscapes of Functional Transitions in Proteins. *Proc. Natl. Acad. Sci. U.S.A.* **2003**, *100*, 12570−12575.
(101) Meinhold, L.; Smith, J. C.; Kitao, A.; Zewail, A. H. Picosecond Fluctuating Protein Energy Landscape Mapped by Pressure−Temperature Molecular Dynamics Simulation. *Proc. Natl. Acad. Sci. U.S.A.* **2007**, *104*, 17261−17265.
(102) Hegler, J. A.; Weinkam, P.; Wolynes, P. G. The Spectrum of Biomolecular States and Motions. *HFSP J.* **2008**, *2*, 307−313.
(103) De Simone, A.; Dhulesia, A.; Soldi, G.; Vendruscolo, M.; Hsu, S.-T. D.; Chiti, F.; Dobson, C. M. Experimental Free Energy Surfaces Reveal the Mechanisms of Maintenance of Protein Solubility. *Proc. Natl. Acad. Sci. U.S.A.* **2011**, *108*, 21057−21062.
(104) LeBard, D. N.; Matyushov, D. V. Glassy Protein Dynamics and Gigantic Solvent Reorganization Energy of Plastocyanin. *J. Phys. Chem. B* **2008**, *112*, 5218−5227.
(105) LeBard, D. N.; Matyushov, D. V. Protein−Water Electrostatics and Principles of Bioenergetics. *Phys. Chem. Chem. Phys.* **2010**, *12*, 15335−15348.
(106) Matyushov, D. V. Nanosecond Stokes Shift Dynamics, Dynamical Transition, and Gigantic Reorganization Energy of Hydrated Heme Proteins. *J. Phys. Chem. B* **2011**, *115*, 10715−10724.
(107) Cascella, M.; Magistrato, A.; Tavernelli, I.; Carloni, P.; Rothlisberger, U. Role of Protein Frame and Solvent for the Redox Properties of Azurin from *Pseudomonas aeruginosa*. *Proc. Natl. Acad. Sci. U.S.A.* **2006**, *103*, 19641−19646.
(108) Wei, J.; Liu, H.; Khoshtariya, D. E.; Yamamoto, H.; Dick, A.; Waldeck, D. H. Electron-Transfer Dynamics of Cytochrome C: A Change in the Reaction Mechanism with Distance. *Angew. Chem., Int. Ed.* **2002**, *41*, 4700−4703.
(109) Khoshtariya, D. E.; Wei, J.; Liu, H.; Yue, H.; Waldeck, D. H. Charge-Transfer Mechanism for Cytochrome *c* Adsorbed on Nanometer Thick Films. Distinguishing Frictional Control from Conformational Gating. *J. Am. Chem. Soc.* **2003**, *125*, 7704−7714.
(110) Waldeck, D. H.; Khoshtariya, D. E. Fundamental studies of long- and short-range electron exchange mechanisms between electrodes and proteins. In *Applications of Electrochemistry and Nanotechnology in Biology and Medicine*; Elias, N., Ed.; Modern Aspects of Electrochemistry Series; Springer: New York, 2011; Vol. *52*, pp 105−241.
(111) Bard, A. J.; Faulkner, L. R. *Electrochemical Methods: Fundamentals and Applications*, 2nd ed.; John Wiley & Sons: New York, 2001; Sections 6.5 and 14.3.
(112) Salimi, A.; Sharifi, E.; Noorbakhsh, A.; Soltanian, S. Immobilization of Glucose Oxidase on Electrodeposited Nickel Oxide Nanoparticles: Direct Electron Transfer and Electrocatalytic Activity. *Biosens. Bioelectron.* **2007**, *22*, 3146−3153.
(113) Chen, X.; Xuan, J.; Jiang, L.; Zhu, J. Preparation of the Glucose Sensor Based on Three-Dimensional Ordered Macroporous Gold Film and Room Temperature Ionic Liquid. *Sci. China Ser. B: Chem.* **2009**, *52*, 1999−2005.
(114) Feng, Z. Q.; Imabayashi, S.; Kakiuchi, T.; Niki, K. Long-Range Electron-Transfer Reaction Rates to Cytochrome *c* across Long- and Short-Chain Alkanethiol Self-Assembled Monolayers: Electroreflectance Studies. *J. Chem. Soc., Faraday Trans.* **1997**, *93*, 1367−1370.
(115) Bond, A. M. *Modern Polarographic Methods in Analytical Chemistry*; Marcel Dekker: New York, 1980; p 27.
(116) Wang, J. H.; Copeland, E. Equilibrium Potentials of Membrane Electrode. *Proc. Natl. Acad. Sci. U.S.A.* **1973**, *70*, 1909−1911.
(117) Cioni, P.; Strambini, G. B. Effect of Heavy Water on Protein Flexibility. *Biophys. J.* **2002**, *82*, 3246−3253.
(118) Chidsey, C. E. D. Free Energy and Temperature Dependence of Electron Transfer at the Metal−Electrolyte Interface. *Science* **1991**, *251*, 919−922.
(119) Smalley, J. F.; Finklea, H. O.; Chidsey, C. E. D.; Linford, M. R.; Creager, S. E.; Ferraris, J. P.; Chalfant, K.; Zawodzinsk, T.; Feldberg, S. W.; Newton, M. D. Heterogeneous Electron-Transfer Kinetics for Ruthenium and Ferrocene Redox Moieties through Alkanethiol Monolayers on Gold. *J. Am. Chem. Soc.* **2003**, *125*, 2004−2013.
(120) Dolidze, T. D.; Khoshtariya, D. E.; Illner, P.; van Eldik, R. Heterogeneous Electron Transfer at Au/SAM Junctions in a Room-Temperature Ionic Liquid under Pressure. *Chem. Commun.* **2008**, 2112−2114.
(121) Khoshtariya, D. E.; Dolidze, T. D.; van Eldik, R. Unusual Mechanism for the Short-Range Electron Transfer within Gold−Alkanethiol−Ionic-Liquid Films of Subnanometer Thickness. *Phys. Rev. E* **2009**, *80*, 065101 (4).
(122) van Eldik, R.; Asano, T.; Le Noble, W. J. Activation and Reaction Volumes in Solution. 2. *Chem. Rev.* **1989**, *89*, 549−688.
(123) van Eldik, R. Electron Transfer Reactions under High Pressure: Application of Spectroscopic and Electrochemical Techniques. *Adv. Chem. Ser.* **1998**, *254*, 315−330.
(124) Swaddle, T. W. Homogeneous Versus Heterogeneous Self-Exchange Electron Transfer Reactions of Metal Complexes: Insights from Pressure Effects. *Chem. Rev.* **2005**, *105*, 2573−2608.

(125) Savéant, J.-M. Single Electron Transfer and Nucleopilic Substitution. *Adv. Phys. Org. Chem.* **1990**, *26*, 1−130.
(126) Khoshtariya, D. E. A Simple Quantum Mechanical Elementary Act Model for S_N2 Nucleophilic Substitution in Aqueous Solutions. *J. Mol. Struct. (THEOCHEM)* **1992**, *255*, 131−144.
(127) Savéant, J.-M. Electron Transfer, Bond Breaking, and Bond Formation. *Acc. Chem. Res.* **1993**, *26*, 455−461.
(128) Cherepanov, D. A.; Krishtalik, L. I.; Mulkidjanian, A. Y. Photosynthetic Electron Transfer Controlled by Protein Relaxation: Analysis by Langevin Stochastic Approach. *Biophys. J.* **2001**, *80*, 1033−1049.
(129) Goguadze, N. G.; Khoshtariya, D. E.; Hammerstad-Pedersen, J. M.; Ulstrup, J. Conformational Dynamics and Solvent Viscosity Effects in Carboxypeptidase-A-Catalyzed Benzoylglycylphenyllactate Hydrolysis. *Eur. J. Biochem.* **1991**, *200*, 423−429.
(130) Shushanyan, M.; Khoshtariya, D. E.; Tretyakova, T.; Makharadze, M.; van Eldik, R. Diverse Role of Conformational Dynamics in Carboxypeptidase A-Driven Peptide and Ester Hydrolyses. Disclosing the "Perfect Induced Fit" and "Protein Local Unfolding" Pathways by Altering Protein Stability. *Biopolymers* **2011**, *95*, 852−870.
(131) Bogatko, S. A.; Bylaska, E. J.; Weare, J. H. First Principles Simulation of the Bonding, Vibrational, and Electronic Properties of the Hydration Shells of the High Spin Fe^{3+} Ion in Aqueous Solutions. *J. Phys. Chem. A* **2010**, *114*, 2189−2200.
(132) Semrouni, D.; Isley, W. C.; Clavaguéra, C.; Dognon, J.-P.; Cramer, C. J.; Gagliardi, L. Ab Initio Extension of the AMOEBA Polarizable Force Field to Fe^{2+}. *J. Chem. Theory Comput.* **2013**, *9*, 3062−3071.
(133) Roach, M. P.; Pond, A. E.; Thomas, M. R.; Boxer, S. G.; Dawson, J. H. The Role of the Distal and Proximal Protein Environments in Controlling the Ferric Spin State and in Stabilizing Thiolate Ligation in Heme Systems: Thiolate Adducts of the Myoglobin H93G Cavity Mutant. *J. Am. Chem. Soc.* **1999**, *121*, 12088−12093.
(134) Decatur, S. M..; Belcher, K. L.; Rickert, P. K.; Franzen, S.; Boxer, S. G. Hydrogen Bonding Modulates Binding of Exogenous Ligands in a Myoglobin Proximal Cavity Mutant. *Biochemistry* **1999**, *38*, 11086−11092.
(135) Liao, M.-S.; Huang, M.-J.; Watts, J. D. Effects of Local Protein Environment on the Binding of Diatomic Molecules to Heme in Myoglobins. DFT and Dispersion-Corrected DFT Studies. *J. Mol. Model.* **2013**, *19*, 3307−3323.
(136) Gavish, B.; Yedgar, S. Solvent viscosity effects on protein dynamics: Updating the concepts. In *Protein−Solvent Interactions*; Gregory, R. B., Ed.; Marcel Dekker: New York, 1995; pp343−373.
(137) Tretyakova, T.; Shushanyan, M.; Partskhaladze, T.; Makharadze, M.; van Eldik, R.; Khoshtariya, D. E. Simplicity within the Complexity: Bilateral Impact of DMSO on the Functional and Unfolding Patterns of α-Chymotrypsin. *Biophys. Chem.* **2013**, *175*, 17−27.
(138) Harvey, J. N. Understanding the Kinetics of Spin-Forbidden Chemical Reactions. *Phys. Chem. Chem. Phys.* **2007**, *9*, 331−343.
(139) Jensen, K. P.; Ryde, U. How O_2 Binds to Heme. Reasons for Rapid Binding and Spin Inversion. *J. Biol. Chem.* **2004**, *279*, 14561−14569.
(140) Liu, Y.-P.; Newton, M. D. Reorganization Energy for Electron Transfer at Film-Modified Electrode Surfaces: A Dielectric Continuum Model. *J. Phys. Chem.* **1994**, *98*, 7162−7169.